Polyfunctionality of broadly reactive non-neutralizing SARS-CoV-2 RBD antibodies

Pierre Rosenbaum[1*], Cyril Planchais[1], Timothée Bruel[2], Maxime Beretta[1], William-Henry Bolland[2], Isabelle Staropoli[2], Florence Guivel-Benhassine[2], Olivier Schwartz[2], and Hugo Mouquet[1, 3*]

[1]Institut Pasteur, Université Paris Cité, Humoral Immunology Unit, Paris, France
[2]Institut Pasteur, Université Paris Cité, CNRS UMR3569, Virus & Immunity Unit, Paris, France

[3]Lead contact

*Correspondence: hugo.mouquet@pasteur.fr (H.M.), pierre.rosenbaum@pasteur.fr (P.R.)

Summary

Persistent SARS-CoV-2 viral escape hindered the search for broad pan-neutralizer monoclonal antibody candidates. To unravel properties of cross-reactive SARS-CoV-2 anti-RBD monoclonal antibodies (mAbs), we identified, cloned, produced, and characterized anti-RBD specific mAbs from convalescent donors infected during the first wave of pandemic. We observed a strong dichotomy between the mAbs based on reactivity profile. A small majority (55%) were poorly cross-reactive but displayed potent neutralization together with strong ADCC, CDC, and ADCP Fc effector functions. In contrast, the others (45%) were broadly cross-reactive, maintaining activity against highly mutated Omicron variants (e.g., BA.2.86, EG.5.1), but lacked neutralization and ADCP, while preserving other Fc-mediated functions. Rare intermediates bridged these groups combining cross-reactivity antiviral potency. Those mAbs were also able to induce SARS-CoV-2 homotrimeric spike conformational changes, increasing anti-FP reactivity and potency. These findings suggest a potential protective role for non-neutralizing, cross-reactive anti-RBD mAbs in mitigating SARS-CoV-2 reinfection.

Introduction

Neutralizing antibodies are central to protection against SARS-CoV-2 infection and reinfection in both vaccinated and convalescent individuals[1–3]. Most target the spike protein (S), particularly the receptor-binding domain (RBD), which dominates serum neutralization[4]. Based on epitope specificity, anti-RBD neutralizers fall into at least four classes, depending on their epitope location - either within (class 1 and 2) or outside (class 3 and after) the receptor-binding motif (RBM)[5–7]. SARS-CoV-2 neutralizing anti-RBD monoclonal antibodies were developed for prophylactic and therapeutic use against COVID-19[8,9]. However, antigenic drift from the continuous SARS-CoV-2 evolution[10,11] severely compromised the reactivity of pre-existing neutralizing antibodies and antibody therapies used in clinics[12–17]. In response, next-generation anti-RBD broadly neutralizing antibodies (bNAbs) more resilient to viral escape such as SA55, VIR-7229 and VYD2311 have been identified and advanced into clinical development[18–20].
Beyond neutralization, monoclonal antibodies with potent Fc-effector functions -such as ADCC, ADCP, and CDC[21–23] - can contribute to SARS-CoV-2 infection control[24–29]. Emerging evidence, including from anti-RBD mAbs like sotrovimab, indicates that these functions may be critical for viral clearance, though their exact role remains to be fully delineated[30–32]. Additionally, anti-RBD antibodies can also exert allosteric effects by inducing conformational changes in the spike protein, mimicking angiotensin converting enzyme 2 (ACE2) interaction, and enhancing the neutralizing potency of anti-FP antibodies[33–35].

To better understand their antiviral properties, we cloned 66 anti-RBD antibodies from IgA and IgG memory B cells of convalescent individuals infected with ancestral SARS-CoV-2. We found that cross-reactive anti-RBD mAbs lacked neutralizing and ADCP activity in comparison with their neutralizing counterparts rapidly escaped by omicron SARS-CoV-2 strains. However, they may retain protective effects through ADCC and CDC Fc-mediated effector function. They also mostly failed to synergize with anti-FP antibodies -either reference or derived from the same patient cohort -likely due to epitope positioning outside the RBM. Notably, we identified a broadly reactive anti-RBD mAb, Cv2R.12145, which synergized with

the anti-FP Cv2F.14107 to enhance neutralization of Omicron BA.1 and BA.5 when combined in a cocktail.

Results

Human anti-RBD memory B-cell antibodies

To select convalescent donors with high anti-RBD seroreactivity for single B-cell antibody cloning, we determined the IgG seroreactivity against SARS-CoV-2 RBD proteins (Wuhan, Beta and Delta variants) of 42 convalescent individuals infected during the first COVID-19 epidemic wave (**Figs. 1A** and **S1A**). Peripheral blood IgG^+ and IgA^+ memory B cells from five selected donors with high anti-RBD cross-reactivity levels were stained with fluorescently labeled RBD Beta (β) and Delta (δ) proteins used as baits for flow cytometry phenotyping and single-cell sorting (**Fig. S1B**). All donors had similar frequencies of RBD-dual binding class-switched memory B-cells ($RBD^{\beta+\delta+}$, 0.11±0.02%; **Figs. 1B** and **S1C**), which were primarily resting memory B lymphocytes ($CD19^+CD27^+CD21^+$) (**Fig. 1C** and **S1D**). From $RBD^{\beta+\delta+}$-capture single B cells, we produced 66 unique anti-RBD monoclonal antibodies (48 IgG and 17 IgA) by recombinant expression cloning[22]. Most of them (85%, n=66 total) showed ELISA cross-reactivity against SARS-CoV-2 Wuhan spike (tri-S), Beta and Delta RBD proteins (**Fig. 1D, S1F** and **Table S1**). Comparison of over 200 immunoglobulin gene features with IgG memory B cells from healthy controls[36] indicated that $RBD^{\beta/\delta}$ antibodies harbored an increased usage of rearranged $V_\lambda6/J_\lambda2$ (P=0.002) and $V_\lambda6$ (P=0.0007) genes, but less rearranged $V_H3/J_\kappa2$ (P=0.006),Jκ2 (P=0.02) and J_H5 (P=0.003) genes as well as IgG2 subclass (P=0.0001) (**Fig. 1E** and **Table S2**). Cross reactive anti-$RBD^{\beta/\delta}$ antibodies were also enriched in CDRH3-negative charges (P=0.02), short CDRλ3 (P=0.01) and had reduced somatic mutations in IgH (5.8 vs. 19.2, P < 0.0001), Igκ (5.9 vs 10.2, P<0.001) and Igλ (5.5 vs 12.4, P<0.0001) (**Fig. 1F** and **Table S2**) as previously reported[37,38]. We compared SARS-CoV-2 antibody repertoires derived from single tri-S[39] or dual $RBD^{\beta/\delta}$ FACS-baiting strategies, assessing specificity, cross-reactivity to pre-Omicron VOCs, and neutralization of D614G (S-fuse assay) (**Fig. S1G**). While overall profiles were similar, dual RBD baiting yielded higher frequencies of cross-reactive mAbs to pre-Omicron VOCs (83.93% vs 52.94%) and Omicron BA.1 (50% vs 29.41%).

Reactivity profiles of SARS-CoV-2 RBD antibodies

To assess cross-reactivity of the 47 anti-RBD specific antibodies, we performed ELISA and flow cytometry using selected SARS-CoV-2 VOC RBDs bearing key escape mutations[12,40,41] (**Fig. 2A** and **S2A**). Apart from the marginal reactivity to SARS-CoV-1 RBD, all of them were SARS-CoV-2 RBD specific and exhibited a low level of polyreactivity (**Fig. S2B**). 44.6% of anti-RBD specific antibodies displayed an almost complete pan-reactivity to omicron VOCs despite being derived from B-cells of patient infected during the first COVID-19 pandemic wave. We classified[6,7] RBD-specific antibodies using ELISA competition assay against Wuhan RBD and reference FDA-approved antibodies (REGN10987[42], CB6[43], LY-CoV555[44], CT-P59[45], COV2-2130[46], ADG-2[47], Ly-CoV1404[13] and S309[48]). Sixteen SARS-CoV-2 RBD antibodies were categorized in G1 (class 1-like), 4 antibodies in G2 (class 2-like), 5 antibodies in G3 (class 3-like) and 22 antibodies in G4 (undetermined) (**Fig. 2B**). We observed that the G1 and G2 groups were enriched with restricted reactivity antibodies (81% and 74) whereas G3 and G4 groups contained a higher proportion of cross-reactive antibodies (60% and 64%) (**Fig. 2, C** and **D;** and **Fig. S2C**).

Antibody features of anti-SARS-CoV-2 RBD antibodies

We then evaluated the neutralizing activity of our RBD-specific antibodies against live viruses[49] using live virus (S-fuse neutralization assay), virus like particles (VLPs) and protein interaction (ELISA-based competition assay)[22]. Only 2 out of the 20 neutralizing mAbs were from the cross-reactive group. At the opposite, they were enriched in the non-neutralizing group (19 out of 27) (**Fig. 3, A-C**). As expected, we also observed that G1 and G4 antibodies were enriched among potent- and non-neutralizers groups, respectively (**Fig. S3, E-G**). Findings were validated by pseudo-neutralization and ELISA blocking assays, though some discrepancies emerged compared to the S-fuse assay. Notably, mAb Cv2R.9102 failed to block ACE2–RBD binding but efficiently neutralized live virus, suggesting an alternative protective mechanism, as previously reported for mAb S309[50]. Conversely, antibodies Cv2R.12118, Cv2R.13207, Cv2R.11116 and Cv2R.11109 efficiently blocked the RBD but not the Tri-S/ACE2 interaction. Given that the Tri-S exhibits a 200-fold higher affinity for the ACE2 receptor compared to the

monomeric RBD domain alone[22], this likely suggest low affinity interactions engaged between these antibodies and their target epitope, which were insufficient to compete and to block the Tri-S binding to ACE2. Of note, most partially neutralizers failed to neutralize Beta and Gamma variants, presumably due to their E484K mutations[51]. We further investigated the neutralizing activity of the neutralizers against an extended panel of post-Omicron VOCs. Six of them neutralized Omicron BA.1 variant using the S-Fuse assay with IC50s below 1.5 µg/ml (**Fig. S3, A-C**). Notably, unlike most reference SARS-CoV-2 antibodies, Cv2R.13162 remained effective against most post-omicron VOCs, including the BQ.1.1 variant, with IC50 below 7 µg/ml (**Fig. S3D**). Next, we evaluated the *in vitro* capacity of the 47 RBD-specific antibodies to promote ADCC (antibody-dependent cellular cytotoxicity), ADCP (antibody-dependent cellular phagocytosis) and complement-dependent cytotoxicity (CDC) through complement deposition readout. The majority of anti-RBD antibodies displayed ADCC and CDC activity regardless of their range of reactivity. In contrast, ADCP activity was strongly associated with antibodies with restricted reactivity, which were also enriched in G1 antibodies (**Fig. 3, D** and **E;** and **Fig. S3H**).

Unmasking property of cross-reactive anti-RBD antibodies

Beyond their intrinsic antiviral properties, anti-RBD antibodies can unmask buried epitopes within S2, as primarily observed with highly neutralizing class I anti-RBD and anti-FP antibodies[33,35]. Given the potential *in vivo* relevance of anti-RBD/anti-S2 synergy, we investigated whether non-neutralizing anti-RBD mAbs, as well as polyclonal anti-RBD antibodies enriched from the same pool of COVID-19 convalescent individuals, could similarly expose the FP epitope. To assess about this cooperation, we identified, cloned, and produced anti-FP specific antibodies from memory B cells originating from two individuals from the same cohort of SARS-CoV-2–infected donors (**Fig.S4, table S3**). Although less representative of the *in vivo* response, reference potent anti-FP antibodies 76E1, CoV4462 and C77G12[33,35,52] were used to guide the selection of two unique anti-FP antibodies, Cv2F.4147 and Cv2F.14107, for their broad cross-reactivity and moderate neutralizing activity. Both antibodies recognized all transiently expressed SARS-CoV-2 spike proteins at the surface of HEK293T cells tested with

an overall higher reactivity of Cv2F.14107 to pre-omicron VOCs, with a peak of expression for the Delta variant (**Fig. 4A**). Only Cv2F.14107 increased its reactivity to SARS-CoV-2 Delta spike following ACE2 binding (**Fig. 4B**) and was used to reveal unmasking capacity of anti-RBD antibodies by flow cytometry (**Fig. 4C**). In line with prior studies[33,35], most unmasking anti-RBD antibodies were significantly enriched the restricted reactivity group. They were also mostly of the G1 and neutralizer group (**Fig. 4, C** and **D;** and **Fig.S5A**). We also identified rare occurrences of non-neutralizers (Cv2R.13148, Cv2R.6151), and cross-reactive antibodies (Cv2R.12145, Cv2R.11176) displaying unmasking properties (**Fig. 4C** and **E**).

Both RBD-enriched and -depleted fractions contained anti-SARS-CoV-2 antibodies and recognized the spike protein from the Delta variant (**Fig. 4F**). However, only the RBD-enriched fractions from five of the six convalescents enhanced the reactivity of the Cv2F.14107 mAb to the SARS-CoV-2 Delta variant. The increased binding of Cv2F.14107 mAb was not observed against the latest highly mutated SARS-CoV-2 BA.2.86 and EG.5 VOCs, most likely due to the low levels or poor unmasking ability of remaining anti-RBD antibodies recognizing these variants (**Fig. S5, B and C**). These findings support that anti-RBD antibodies can mediate FP unmasking *in vivo* in SARS-CoV-2–infected or vaccinated individuals. As an overview, principal component analysis (**Fig. 4G**) revealed a clear segregation between restricted anti-RBD, and cross-reactive antibodies based on effector functions, neutralization, and unmasking capacity. Thus, anti-RBD antibodies tend to be either highly cross-reactive or show strong antiviral functions, but rarely both.

Cooperative neutralization of Cv2R.12145 and Cv2F.14107

Cv2R.12145 is one of the rare cross-reactive antibodies which also neutralizes pre-omicron SARS-CoV-2 Wuhan and delta VOCs with IC50 ranging from 0.3 to 0.7 µg/mL, respectively (**Fig.5, A** and **B**). The Cv2R.12145 monoclonal antibody unmasked FP epitopes as effectively as ACE2 or the ACE2-mimicking CB6 reference mAb[35,53] (**Fig. 5C** and **Fig. S5D**). CB6 lost unmasking capacity against XBB.1.5, EG.5.1 and BA.2.86 due to reduced reactivity (**Fig.5C**). Cv2R.12145 was also tested alongside other cross-reactive RBD antibodies with unmasking

properties against these variants and consistently enhanced anti-FP Cv2F.14107 reactivity (**Fig. S6**). Finally, we evaluated the synergistic effects of antibody cocktail made of Cv2R.12145 and Cv2F.14107 in terms of neutralization (**Fig. 6D** and **E**). We found that the Cv2R.12145 - Cv2F.14107 combination exhibited superior *in vitro* neutralization than single antibodies against XBB.1.5 (pseudoneutralization assay) and EG.5 (S-fuse assay) (total synergy δ-score of 4.15 and 2.20, respectively, while a global synergy δ-score would range from −10 to 10). Antibodies acted particularly synergistically at specific concentrations (local synergy δ-score of 7.4 for BA.5 in the range of 50–200 μg/mL and 3.12-12.5 μg/mL for Cv2F.14107 and Cv2R.12145, respectively; local synergy δ-score of 4.25 forEG.5 in the range of 50–200 μg/mL and 2.5-10 μg/mL for Cv2F.14107 and Cv2R.12145, respectively) (**Fig. 6D** and **E**).

Discussion

Monoclonal antibodies targeting the RBM are among the most potent SARS-CoV-2 neutralizers, as they block RBD/ACE2 interaction[37]. However, the strong immune pressure on this site has driven escape mutations that confer resistance to neutralization—including by FDA-approved antibodies[17,54–56], thereby compromising both vaccine and therapeutic antibody efficacy. One of the common strategies used to overcome viral escape consist in the targeting of epitopes that are conserved throughout viral evolution[57,58]. However, resilience of viral sequences frequently results from low immune pressure rather than structural or functional constraints[59,60].

Consistent with previous report[61], we found that using the RBD-baiting strategy with different SARS-CoV-2 variants to isolate antigen-specific B cells could facilitate the identification of cross-reactive antibodies. Here, we characterized 47 anti-RBD specific antibodies derived from circulating memory B cells generated during the first SARS-CoV-2 pandemic based on their reactivity profile against SARS-CoV-2 variants. Twenty-one of them bound up to BA.2.86 variant. Most belonged to the undefined RBD-class G4, suggesting a preference for non-neutralizing epitopes that are under lower selective pressure. Despite their poor neutralization and limited ADCP activity, these cross-reactive RBD-specific antibodies retained the ability to induce CDC and ADCC, potentially contributing to protection against SARS-CoV-2 infection[23,62–64]. CDC can indeed facilitate the clearance of SARS-CoV-2-infected cells through pore formation on their surface[65,66], but may also exacerbate COVID-19 severity by triggering the release of C3a and C5a anaphylatoxins, which contribute to respiratory distress syndrome, coagulopathy, and inflammatory response[67–69]. Conversely, both ADCC and ADCP have been shown to strongly protect against COVID-19 severe disease, notably in vaccinated patients[24,70–72]. Combinations of antibodies targeting non-overlapping epitopes is a widely developed strategy to overcome immune escape imposed by HIV-1, Ebola, influenza, or SARS-CoV-2 viruses[73–76]. In addition, although synergistic effects between two antibodies have been rarely reported, they may play a significant role in human protection, as already shown in Marburg or Ebola infections[77–79]. In the context of SARS-CoV-2 infection, previous

studies have shown that ACE2-mimicking anti-RBD neutralizing antibodies can enhance anti-FP reactivity by inducing spike conformational changes[33,80]. In this study, we show that cross-reactive SARS-CoV-2 antibodies are poor inducers of FP exposure likely due to their binding outside the RBM region of the Spike protein. Beyond non-neutralizing antibodies, we also identified a rare broadly reactive class 1-like mAb (Cv2R.12145), that strongly binds to the SARS-CoV-2 RBD up to the BA.2.86 variant but progressively losing its neutralizing capacity beyond BA.1, with potent ACE2-mimicking properties. We demonstrated that combining Cv2R.12145 mAb with an anti-FP mAb (Cv2F.14107) could enhance antiviral immunity by increasing both reactivity and potency. Whether the ACE2-mimicking properties of anti-RBD antibodies play a crucial role in viral clearance *in vivo* remains unknown and should be investigated.

Altogether, our results highlight the challenge of identifying ultrapotent neutralizing antibodies targeting the RBD, given the continuous emergence of new SARS-CoV-2 variants. Cross-reactive anti-RBD antibodies severely lacked neutralizing and effector functions. Unlike anti-RBD antibodies with limited cross-reactivity, these antibodies retain recognition of mutated SARS-CoV-2 variants, can undergo maturation, and may play a role in the control of reinfection by engaging ADCC and CDC effector functions. Whether this role is negligible, beneficial, or deleterious remains to be answered.

Acknowledgments

We are grateful to all convalescent donors who consented to be part of this study, as well as all investigators, clinicians, medical staff members, and participants involved in the study. The French COVID Cohort, sponsored by the Institut national de la santé et de la recherche médicale (INSERM), is funded through the REACTing (REsearch & ACtion emergING infectious diseases) consortium, the Ministry of Health and Social Affairs, the Ministry of Higher Education and Research dedicated COVID-19 fund and Programme hospitalier de recherche clinique no. 20- 0424. Funding sources are not involved in the study design, data acquisition, data analysis, data interpretation or manuscript writing. This work was supported by grants

from the Agence Nationale de la Recherche REACTing COVID-19 (#20RR028-00), the European Commission Horizon 2020 program (RECoVER project, #101003589), the Institut Pasteur Task Force COVID-19 (2019-NCOV THERAMAB project), the Fondation de France (#00106077), and partly by a SpikImm-Institut Pasteur R&D program. H. Mouquet also received core funding from the Institut Pasteur and INSERM. This work was also supported by a Pasteur-Roux-Cantarini fellowship of Institut Pasteur. We thank CBUtechs platform for their support in experiments involving flow cytometry. We also thank Lubka Romenina for providing pre-SARS-CoV-2 pandemic serum for complement study.

Author contributions

H. Mouquet conceived and supervised the study. P. Rosenbaum, C. Planchais, T. Bruel, M. Beretta, WH. Bolland, I. Staropoli, F. Guivel-Benhassine, and O. Schwartz, H. Mouquet performed and/or analyzed the experiments. P. Rosenbaum, C. Planchais, T. Bruel and H. Mouquet wrote and corrected the manuscript.

Figure legends

Figure 1. SARS-CoV-2 RBD–specific memory B-cell sorting and antibody cloning from COVID-19 convalescent individuals.

(**A**) 3D plot of seroreactivity against RBD Wuhan, Beta, and Delta. Circled dots correspond to samples selected for memory-B cell FACs sorting. Dots are color-coded according to the areas under curve (AUCs) obtained from OD_{405nm} ELISA seroreactivity titration scaling from blue (low reactivity) to red (high reactivity) from COVID-19 convalescents (n=42).

(**B**) Flow-cytometric plots showing the SARS-CoV-2 dual $RBD^{\beta+\delta+}$ binding of IgG+ and IgA+ memory B cells (gated as indicated on Fig.S1B) in blood from 5 COVID-19 convalescents.

(**C**) Scatter plot with mean of the distribution of total (black) and SARS-CoV-2 $RBD^{\beta+\delta+}$ (blue) IgG^+ and IgA^+ memory B-cell subsets (n = 5). $CD19^+$ B cell subsets are gated as indicated in Fig.S1B and then characterized as follows: B_{IM} (intermediate memory, $CD27^-CD21^+$), B_{RM} (resting memory $CD27^+CD21^+$), B_{AM} (activated memory, $CD27^+CD21^-$), and B_{TLM} (tissue-like memory $CD27^-CD21^-$). Groups were compared by Mann-Whitney test (P≤0.06 only are shown).

(**D**) Bubble plot of human IgG antibodies reactivity cloned from SARS-CoV-2 $RBD^{\beta+\delta+}$ IgG^+ and IgA^+ memory B cells from COVID-19 convalescents. Reactivity has been measured in ELISA using OD_{405nm} against RBD Delta (x axis), RBD Delta (y axis) and tri-S Wuhan (bubble size). Antibodies were split between cross (yellow; >1 OD_{405nm} for both RBD β and RBD δ), single (black; >1 OD_{405nm} for one of RBD β or RBD δ), and no reactivity (gray; <1 OD_{405nm} for both RBD Beta and RBD Delta), data available on table S1.

(**E**) Volcano plot analysis comparing the immunoglobulin gene repertoire of IgG+ memory B cells from healthy individuals (left side; IgG.mB, unexposed to SARS-CoV-2[36]) from SARS-CoV-2 $RBD^{\beta+\delta+}$ IgG+/IgA+ B cells from COVID-19 convalescents (right side). Δmean (x axis) represents mean difference for each parameter between both groups. Blue dots indicate statistically significant differences between both Ig gene repertoires coupled |Δmean|≥1.2. p-values (y axis) calculated by Fischer test. Data available on table S2

(**F**) Violin plots comparing the number of mutations in V_H, V_κ, and V_λ genes of control IgG+ memory B cells from unexposed healthy individuals[36] (black; n = 27) and SARS-CoV-2 $RBD^{\beta+\delta+}$–specific (blue; n = 18). Representation shows median±quartiles. Numbers of mutations were compared across groups of antibodies using Mann-Whitney test. ****, P < 0.0001; ***, P < 0.001; **, P < 0.01; *, P < 0.05. Data available on table S2

Figure 2. Neutralizing activity of omicron reactive RBD-specific antibodies and epitope mapping.

(**A**) Heatmap showing human RBD Beta- and Delta- specific antibodies (n = 47) reactivity on ELISA against purified recombinant tri-S, S1, and RBD SARS-CoV-2 Wuhan and subsequent variants antigens. Cells are color-coded according to the mean of duplicates OD_{405nm} values with 1µg/mL of mAb, blue colors indicating strongest reactivities. Antibodies were split in four reactivity groups: Cross-reactive (red) for antibodies not showing a reactivity below 2 OD_{405nm} for more than three omicron variants antigens; restricted reactivity (grey) for the other antibodies. Graphic on the right side represents percentage of reactive antibodies (OD_{405nm}> 2) per antigen for total (black), cross- (red), and restricted (gray) reactive antibodies groups. Data available on table S1.

(**B**) Heatmap of ELISA competition between anti-RBD and reference antibodies for RBD Wuhan antigen. Cells are color-coded according to the mean of duplicates percentage of competition based on OD_{405nm} values, with blue colors indicating strongest competitions. Reference antibodies were divided into four group based on literature: G1 | Class 1-like (red) for CT-P59[45,81], Cv2.1169[22], and CB6[53,81]; G2 | Class 2-like (yellow) for LyCoV555[81,82]; G3 | Class 3-like (blue) for REGN10987[81,82], LyCoV1404[81,83], CoV2-2130[46,81] and S309[81,83,84]; Class 4 (black) for ADG-2[47]. Anti-RBD antibodies were split in four groups: G1 | Class 1-like (red) for antibodies competing above 30% with CB6; G2 | Class 2-like (yellow) for remaining antibodies competing above 30% with class 2 reference mAb (LyCoV555) and less than 30% competition with class 1 reference antibodies; G3 | Class 3-like (blue) for remaining antibodies competing

above 60% for at least one class III antibodies and less than 30% competition with class 2 reference antibodies, ; G4 | undefined (gray) for remaining antibodies corresponding for none of the previous criteria. Data available on table S1.
(**C**) Pie chart representing the percentage of cross- (red), and restricted- reactive (grey) antibodies for each G1, G2, G3 and G4 groups (as indicated on Fig.2B). Value at the center corresponds to total mAb amount for each group.
(**D**) Graphical representation of RBD-specific antibodies reactivity against SARS-CoV-2 Wuhan and Omicron subvariants. Antibodies were split in G1 (red); G2 (yellow); G3 (blue) and G4 (gray) groups based on the strategy described in Fig.2B. Antibodies were considered as reactive against a parameter when OD_{405nm} exceeded 2. The percentage of reactive antibodies (y axis) was determined by the ratio between reactive antibodies and total amount of antibodies for each group. Data available on table S1.

Figure 3. Potency and Fc-mediated effector function of SARS-CoV-2 RBD–specific antibodies
(**A**) Heatmap of human RBD-specific antibodies neutralizing reactivity against SARS-CoV-2 D614G, Alpha, Beta, Gamma, Delta variants using S-fuse, Virus-like particles (VLP) pseudo neutralization assay, and/or ACE2/tri-S|RBD block ELISA assay, with blue colors indicating strongest inhibition percentages. Values correspond to mean of duplicates. Antibodies were split in three groups: Pan-neutralizer (dark pink) for antibodies showing at least 40% neutralization for all SARS-CoV-2 D614G, Alpha, Beta, Gamma, Delta S-fuse assays; Partial neutralizer (pink) for antibodies showing a reactivity above 80% neutralization for at least one parameter among D614G, Alpha, Beta, Gamma, Delta S-fuse; Non-neutralizer (white) for the other antibodies. Reactivity color coding below corresponds to mAb reactivity group described on Fig 2A. Data available on table S1.
(**B**) Graphical representation of RBD-specific antibodies neutralizing activity in S-Fuse, VLP, and ACE2/tri-S|RBD block assays. Antibodies were grouped based on G1 (red; G2 (yellow); G3 (blue) and G4 (gray) based on the strategy described in Fig.2B antibodies were considered as positive for a given parameter when inhibition/neutralization values were above 50% (data available on table S1). The percentage of neutralizing antibodies (y axis) was determined by the ratio between positive antibodies and total amount of antibodies for each group.
(**C**) Histogram showing ADCC, CDC, and ADCP score of each anti-RBD antibody, ordered by reactivity group described in Fig.2A (cross- (red), and restricted- reactive (grey)). Dotted bar represents the basal value with negative control. Data represents the mean± SD of duplicates from two independent experiments.
(**D**) Scatter plot with means of ADCC, ADCP, and CDC functions of cross- (red; n=21) and restricted- reactive (gray; n=26) SARS-CoV-2 RBD specific antibodies groups as described in Fig.2A. Scores were compared across groups of antibodies using Mann-Whitney's test. ****, $P < 0.0001$; ***, $P < 0.001$; **, $P < 0.01$; *, $P < 0.05$.

Figure 4. Anti-RBDs potentialize anti-FP Cv2F.14107 reactivity
(**A**) Graph showing reactivity of anti-FP Cv2F.4147 (blue) and Cv2F.14107 (dark red) antibodies by flow cytometric assay on HEK293F cells expressing tri-S from different SARS-CoV-2 variants or none (mock). Data represent mean±SD of duplicate values of geometric mean fluorescence intensities (gMFI) fold increase vs. no mAb.
(**B**) Overlay panel (left) and histogram (right) of fluorescence intensity of Cv2F.4147 (blue) and Cv2F.14107 (dark red) antibodies in presence or absence of ACE2 by flow cytometric assay on HEK293F cells expressing tri-S from SARS-CoV-2 Delta (left panel). One representative overlay panel out of two is shown. Histogram (right panel) shows the mean±SD of duplicate values of fold increase of gMFI AUC vs. no mAb.
(**C**) Histogram showing reactivity increase of Cv2F.14107 by anti-RBDs on HEK293F tri-S delta SARS-CoV-2 transfected cells. Black dotted line represents basal value of fold increase of gMFI. Blue dotted line represents two times the basal gMFI value. Data represent the mean±SD of duplicates. Data are ordered from highest to lowest unmasking anti-RBD mAb,

with color-coding based on reactivity cross- (red) and restricted- (gray) reactivity groups described on Fig.2A and references (pink), non-anti-RBDs (green), and controls (black).
(**D**) Scatter plot with means of increased Cv2F.14107 reactivity measured on HEK293F tri-S delta SARS-CoV-2 transfected cells of cross- (red; n=21) and restricted- reactive (gray; n=26) SARS-CoV-2 RBD specific antibodies groups described on Fig.2A. Fold increase vs no antibodies were compared across groups of antibodies using Mann-Whitney's test. ****, $P < 0.0001$; ***, $P < 0.001$; **, $P < 0.01$; *, $P < 0.05$.
(**E**) Pie chart representing proportion of high (blue >2 FI_{gMFI}) and low (gray ≤2 FI_{gMFI}) anti-FP reactivity increase, and anti-RBD mAb per reactivity group. Value at the center corresponds to total mAb amount for each group.
(**F**) Histogram showing reactivity (left) and Cv2F.14107 reactivity increase (right) of polyclonal RBD (blue) and non-anti RBD (gray) antibodies purified from individual COVID-19 convalescent serum on HEK293F tri-S delta SARS-CoV-2 transfected cells. Mean±SD of duplicate values are shown.
(**G**) PCA 2D-plot showing the antiviral-related variables (arrows) discriminating against anti-RBD antibodies (n = 47). Each dot represents a single mAb, color coded based on groups described on Fig.2A (cross-(red) restricted- (gray) reactivity).

Figure 5. Reactivity and potency of Cv2R.12145 or Cv2F.14107 against mutated SARS-CoV-2 variants
(**A**) Reactivity curves of SARS-CoV-2 Delta and subsequent Omicron variants by Cv2R.12145 anti-RBD mAb by ELISA titration assay. Dots and error bars indicate the mean±SD of duplicate values. Nonlinear modelization was calculated by four parameter inhibitor concentration vs. response regression fit.
(**B**) Neutralization curves of SARS-CoV-2 D614G, Delta and subsequent Omicron variants by the Cv2R.12145 anti-RBD mAb by S-Fuse neutralization assay. Dots and error bars indicate the mean±SD of duplicate neutralization percentage values from 2 independent experiments. Nonlinear modelization was calculated by four parameter inhibitor concentration vs. response regression fit.
(**C**) Overlay representation (left) and histogram (right) of anti-RBD reactivity and Cv2F.14107 reactivity fold increase vs. no mAb of Cv2R.12145 (blue); CB6 (red), and ACE2 (gray) and no aRBD (light gray) controls. Flow cytometric assay on HEK293F cells expressing tri-S from SARS-CoV-2 Delta variant. One representative overlay out of two is shown. Histograms show mean±SD of duplicates values.
(D) Heatmap (left) and area if synergy representation (right) evaluating the synergy between Cv2F.14107 and Cv2R.12145 on pseudo-neutralization assay for BA.5 variant. For the heatmap, darker blue colors correspond to higher neutralization percentage. Values represented are means of duplicates. For the graphical representation, anti-synergistic effect scale to low delta score in green to high delta score in red. Square in blue represents the highest synergy area and associated delta score.
(E) Heatmap (left) and area if synergy representation (right) evaluating the synergy between Cv2F.14107 and Cv2R.12145 on live virus S-Fuse assay for EG.5 variant. For the heatmap, darker blue colors correspond to higher neutralization percentage. Values represented are means of duplicates. For the graphical representation, anti-synergistic effect scale to low delta score in green to high delta score in red. Square in blue represents the highest synergy area and associated delta score.

Lead Contact
Requests for resources and reagents should be directed to and will be fulfilled by the lead contact, Hugo Mouquet (hugo.mouquet@pasteur.fr).
Materials Availability
Requests for reagents will be made available by the lead contact with a Material Transfer Agreement.
Data and Code Availability
This paper does not report original code. Data used for the analysis is available in supplemental tables. Any additional information required to reanalyze the data reported in this paper is available from the lead contact upon reasonable request.

EXPERIMENTAL MODEL AND SUBJECT DETAILS

Human samples
Human blood samples were obtained from Wuhan COVID-19 convalescent donors which were part of the CORSER and French COVID cohorts in accordance with and after ethical approval from all the French legislation and regulation authorities. The CORSER study was registered with ClinicalTrials.gov (NCT04325646). The CORSER and French COVID studies both received ethical approval by the regional investigational review board (Comité de Protection des Personnes Ile-de-France, Paris, France) and performed according to the European guidelines and the Declaration of Helsinki. All participants gave written consent to participate in this study, and data were collected under pseudo-anonymized conditions using subject coding.

Viruses
SARS-CoV-2 BetaCoV/France/IDF0372/2020 (GISAID ID: EPI_ISL_406596) and D614G (hCoV-19/France/GE1973/2020; GISAID ID: EPI_ISL_414631) strains were supplied by the National Reference Centre for Respiratory Viruses (Institut Pasteur[86,87]). α (B.1.1.7; GISAID ID: EPI_ ISL_735391), β (B.1.351; GISAID ID: EPI_ISL_964916), δ (B.1.617.2; GISAID ID: EPI_ISL_2029113), BA.1 (GISAID ID: EPI_ISL_6794907), BA.2 (GISAID ID: EPI_ISL_10654979), BA.5 (GISAID ID: EPI_ISL_13660702), BA.2.75.2 (GISAID accession ID: EPI_ISL_15731524), BA.4.6 (GISAID ID: EPI_ISL_15729633, BQ.1.1 (GISAID ID: EPI_ISL_15731523, XBB.1 (GISAID ID: EPI_ISL_15619797), XBB.1.5 (GISAID ID: EPI_ISL_1635849) strains were provided by the Virus and Immunity Unit (Institut Pasteur[85,87–89]). The γ variant (P.1.; hCoV-19/Japan/TY7-501/2021; GISAID ID: EPI_ISL_833366) was obtained from Global Health security action group Laboratory Network[90]. Viruses were amplified by one or two passages in Vero E6 cell cultures and titrated. The sequence of the viral stocks was verified by RNAseq.

METHOD DETAILS
Expression and purification of viral proteins
Synthetic fusion peptide sequences (GenScript Biotech) are provided in table S3.
Codon-optimized nucleotide fragments encoding stabilized versions of SARS-CoV-2 , SARS-CoV-1, MERS-CoV, HKU1-CoV, 229E-CoV, OC43-CoV, SARS-CoV-2 BA.1 spike (HexaPro; S_6P; S) ectodomains, and SARS-CoV-2 S2, S2 depleted from FP, HR2, or SH domain, followed by a Foldon trimerization motif and C-terminal tags (8xHis-tag, Strep-tag, and AviTag) were synthesized and cloned into pcDNA3.1/Zeo(+) expression vector (Thermo Fisher Scientific).
Synthetic nucleotide fragments coding for SARS-CoV-2 RBD Wuhan, BA.1, BA.2, BA.2.12.1, BA2.75, BA2.75.2, BA.3, BA4/5, BA4.6, BF.7, BQ.1, BQ.1.1, XBB.1, XBB.1.16, XBB.1.5, BA.2.86, followed by C-terminal tags (8xHis-tag, Strep-tag, and AviTag), as well as human ACE2 (plus 8xHis- and Strep-tags) were cloned into the pcDNA3.1/Zeo(+) vector.
Glycoproteins were produced by transient transfection of exponentially growing Freestyle 293-F suspension cells (Thermo Fisher Scientific) using polyethylenimine (PEI) precipitation method, as previously describbed[91]. Proteins were purified from culture supernatants by high

performance chromatography using the Ni Sepharose Excel Resin according to the manufacturer's instructions (GE Healthcare), dialyzed against PBS using Slide-A-Lyzer dialysis cassettes (Thermo Fisher Scientific), quantified using NanoDrop 2000 instrument (Thermo Fisher Scientific). AviTagged tri-S and RBD proteins were biotinylated using BirA biotin–protein ligase bulk reaction kit (Avidity) or Enzymatic Protein Biotinylation Kit (Sigma-Aldrich) following manufacturer's instructions. Non-AviTagged protein (ACE2, antibodies) were biotinylated using EZ-Link Sulfo-NHS-Biotin kit (Thermo Scientific) following manufacturer's instructions.
For flow cytometry RBD single B-cell FACs sorting, biotinylated SARS-CoV-2 RBD Beta and Delta protein were coupled extemporaneously with respectively streptavidin R-PE and streptavidin APC (Thermo Fisher Scientific). For flow cytometry FP single B-cell FACs sorting, biotinylated FP (KRSFIEDLLFNKVTLADAGFIK; GenScript Biotech) was coupled extemporaneously with streptavidin R-PE or streptavidin APC (Thermo Fisher Scientific).

Flow cytometry immunophenotyping
PBMCs were isolated from donors' blood using Ficoll Plaque Plus (GE Healthcare). Human B cells were first isolated from donors' PBMCs by MACS using human CD19 MicroBeads (Miltenyi Biotec) following manufacturer's procedures. Enriched B cells were then incubated for 30 min at 4°C with an extemporaneously prepared mix of biotinylated SARS-CoV-2 RBD Beta and Delta protein coupled with respectively streptavidin R-PE and streptavidin APC (Thermo Fisher Scientific). Cells were then washed once with 1% FBS-PBS (FACS buffer) and incubated for 30 min at 4°C. For RBD positive B-cells FACs sorting (using a FACS Aria Fusion Cell Sorter (Becton Dickinson)), $CD19^+$ B cells were then stained using LIVE/DEAD aqua fixable dead cell stain kit (Molecular Probes; Thermo Fisher Scientific) to exclude dead cells. Antibody mix was then added on cells with a cocktail of mouse anti-human antibodies: CD19 Alexa 700 (HIB19; BD Biosciences), CD21 BV421 (B-ly4; BD Biosciences), CD27 PE-CF594 (M-T271; BD Biosciences), IgG BV786 (G18-145; BD Biosciences), IgA FITC (IS11-8E10; Miltenyi Biotec), IgD APC-H7 (IA6-2; BD Biosciences). For FP positive B-cells FACs sorting for CC4 (or FC27) donor using a FACS Aria Fusion (or Symphony S6 Cell Sorter (Becton Dickinson)), $CD19^+$ B cells were stained using LIVE/DEAD aqua fixable dead cell stain kit (Molecular Probes; Thermo Fisher Scientific) to exclude dead cells. Antibody mix was then added on cells with a cocktail of mouse anti-human antibodies: CD19 Alexa 700 (HIB19; BD Biosciences), CD21 BV711 (or BV421; B-ly4; BD Biosciences), CD27 PE-CF594 (M-T271; BD Biosciences), IgG BV786 (G18-145; BD Biosciences), IgA FITC (IS11-8E10; Miltenyi Biotec), and β7 integrin BV421 (or BUV395; FIB504, BD Biosciences).
Cells were then washed and resuspended in FACS buffer. Following doublet exclusion, living lymphoid cells were selected and gated using $CD19^+$ marker. Non-IgA and -IgG were then excluded and double RBD (or FP) positive cells were sorted. Analysis were done by FlowJo software (v10.8; FlowJo LLC).

Single B-cell FACS sorting and expression-cloning of antibodies.
Peripheral blood human B cells were isolated and stained as described above. Double positive SARS-CoV-2 $RBD\beta^+\delta^+$ or FP IgG+ and IgA+ B cells were sorted one by one into 96-well PCR plates. Single-cell cDNA synthesis using SuperScript IV reverse transcriptase (Thermo Fisher Scientific) followed by nested-PCR amplifications of IgH, Igκ, and Igλ genes, and sequences analyses for Ig gene features were performed as previously described[36,92]. Purified digested PCR products were cloned into human Igγ1-, Igκ-, or Igλ-expressing vectors (GenBank# LT615368.1, LT615369.1, and LT615370.1, respectively), as previously described[92]. Recombinant antibodies (and Cv2.1169) were produced by transient co-transfection of Freestyle 293-F suspension cells (Thermo Fisher Scientific) using the PEI precipitation method, as previously[91]. Recombinant human IgG1 antibodies were purified by affinity chromatography using Protein G Sepharose 4 Fast Flow (GE Healthcare). Purified antibodies were dialyzed against PBS. The purified parental IgG1 antibody versions of benchmarked RBD antibodies (REGN10987[42], CB6[43], LY-CoV555[44], CT-P59[45], COV2-2130[46], ADG-2[47], Ly-CoV1404[13] and S309[48] and FP antibodies (C77G12[33], 76E1[35], CoV44-62[52]) were prepared as

described above after cloning of synthetic DNA fragments (GeneArt; Thermo Fisher Scientific) coding for the immunoglobulin variable domains. Recombinant human IgG1 antibodies were purified by affinity chromatography using Protein G Sepharose 4 Fast Flow (GE Healthcare). Purified digested PCR products from Cv2F.4147, Cv2F.14107 and 76E1 were also cloned into human Igα1, or vectors Fab-Igγ1-expressing vector[91].Recombinant human IgA antibodies and Fab were purified by affinity peptide M-coupled agarose beads (Invivogen) and Ni Sepharose® Excel Resin (GE Healthcare), respectively.

ELISAs

ELISAs were performed as previously described[93,94]. Briefly, high-binding 96-well ELISA plates (Costar; Corning) were coated overnight with purified recombinant Coronavirus proteins. After washings with 0.05% Tween 20-PBS (washing buffer) using hydroSpeed microplate washer (Tecan), the plates were blocked for 2 h with 2% BSA, 1 mM EDTA, 0.05% Tween 20-PBS (Blocking buffer), washed, and incubated with serially diluted human sera, antigens or recombinant antibodies in PBS. After washings, the plates were incubated for 30 or 60 min with anti IgG HRP-conjugated antibody (Jackson), washed again, and revealed by addition of 100µL of horseradish peroxidase chromogenic substrate (ABTS solution ; Euromedex). Optical densities were measured at 405 nm (OD405nm) using sunrise microplate absorbance reader (Tecan). To test ELISA binding, SARS-CoV-2 antigens and variants were coated with 125 ng/well. Recombinant IgG1 RBD antibodies were tested at 1 µg/ml. Antigen reactivity titrations were performed for the six most potent antibodies were tested at 10µg/ml followed by seven consecutives 1:4 dilutions in PBS. Recombinant IgG1 FP antibodies were tested at 10 µg/ml. followed by seven consecutives 1:10 dilutions in PBS.

For the tri-S/RBD vs. ACE2 blocking experiments, ELISA plates (Costar; Corning) were coated overnight with 250 ng/well of purified ACE2 ectodomain and washed and blocked as described above. For non-Omicron variants, recombinant IgG1 antibodies were incubated at 20 µg/ml in presence of biotinylated RBD in PBS at 2 µg/ml, or at 2 µg/ml in presence of biotinylated tri-S in PBS at 1 µg/ml. For Omicron variants, recombinant IgG1 antibodies were incubated at 200 µg/ml in presence of biotinylated RBD in PBS at 2 µg/ml. Recombinant IgG1 antibodies were incubated at 10 µg/ml in presence of biotinylated tri-S in PBS at 1 µg/ml or After washings, the plates were revealed by incubation for 30 min with streptavidin HRP-conjugated protein (BD Biosciences). Percentage of blocking was calculated as followed ($100*(mGO53_{OD405nm} – RBD_{OD405nm}$ in presence of mAb competitor)/ $mAb_{OD405nm}$) . Negative values were considered à 0.

For competition ELISAs, 250 ng/well of RBD Wuhan protein was coated on ELISA plates (Costar; Corning). After washings and blocking steps described above, plates were then incubated for 2 h with biotinylated antibodies at a concentration of 25 ng/ml in presence of recombinant IgG1 antibodies at 50µg/ml. Plates were developed using HRP-conjugated streptavidin (BD Biosciences) as described above. Percentage of competition was calculated as followed ($100*(mGO53_{OD405nm}$ – reference $mAb_{OD405nm}$ in presence of mAb competitor)/ $mAb_{OD405nm}$)). Negative values were considered à 0.

Polyreactivity ELISA was performed as previously described[95,96]. Briefly, high-binding 96-well ELISA plates were coated overnight with 500 ng/well of purified double-stranded DNA, KLH, LPS, peptidoglycan or 250 ng/well of insulin (Sigma-Aldrich). After blocking and washing with 0.001% Tween 20-PBS steps, recombinant IgG antibodies were tested at 4 µg/ml and three consecutive 1:4 dilutions in PBS for anti-FPs and at 10 µg/ml and three consecutive 1:10 dilutions in PBS for anti-RBDs. Control antibodies, mGO53[96] (negative), and ED38[97] (high positive) were included in experiments.

For peptide-ELISA used for assays with FP, high-binding 96-well ELISA plates were coated overnight with 1 µg/well of FP. After blocking (with 5% sucrose, 3% milk, 1% Tween 20) and washing with 0.1% Tween 20-PBS steps, antibodies were tested at 10 µg/ml and three consecutive 1:10 dilutions in PBS with 1% BSA and 0.1% tween 20.

Flow cytometry binding assay

SARS-CoV-2 specificity validation of cloned human IgG antibodies was performed using the S-Flow assay as previously described[86]. To evaluate spike cross-reactivity, Freestyle 293-F were transfected with pUNO1-Spike-dfur expression vectors (Spike and SpikeV1 to V13 plasmids; Invivogen; 1.2 µg plasmid DNA per 10^6 cells) or with pHCMV expression vectors (for XBB.1.5, BA.2.86, EG.5.1; Virus and Immunity unit[98]; 1.2 µg plasmid DNA per 10^6 cells) using PEI-precipitation method. 48 h after transfection. For HEK293-F recognition by antibodies 0.3 × 10^6 transfected and non-transfected control cells were incubated with IgG antibodies for 30 min at 4°C (1 µg/ml). After washings, cells were incubated for 20 min at 4°C with AF647-conjugated goat anti-human IgG antibodies (1:1,000 dilution; Thermo Fisher Scientific) and LIVE/DEAD Fixable Viability dye Aqua (1:1,000 dilution; Thermo Fisher Scientific), washed and resuspended in PBS–paraformaldehyde 1% (Electron Microscopy Sciences).
For anti-FP reactivity increase (and associated mAb reactivity) by anti-RBD antibodies or ACE2 evaluation, 0.3 × 10^6 transfected and non-transfected control cells were incubated by 10µg/mL anti-RBD antibodies or controls in presence of 10 µg/mL Dy650 labeled-ACE2 or anti-FP antibodies in a total volume of 100µL of PBS supplemented with 5% FBS and 2mM EDTA for 2 hours at room temperature[33,34]. After PBS washing, cells were incubated for 20 min at 4°C with AF647-conjugated goat anti-human IgG antibodies (1:1.000 dilution; Thermo Fisher Scientific) and LIVE/DEAD Fixable Viability dye Aqua (1:1.000 dilution; Thermo Fisher Scientific), washed and resuspended in PBS–paraformaldehyde 1% (Electron Microscopy Sciences).
Antibodies or ACE2 labeling with Dy650 was performed using Dylight 650 NHS ester kit (Thermo Scientific) following manufacturer instructions.
Data were acquired using a CytoFLEX flow cytometer (Beckman Coulter) and analyzed by FlowJo software (v10.8; FlowJo LLC). Fold-increase was considered as the ratio between tested sample gMFI-APC and the same condition without mAb.

SARS-CoV-2 S-Fuse neutralization assay
S-Fuse cells (U2OS-ACE2 GFP1-10 or GFP 11 cells) were mixed (ratio 1:1) and plated at a density of 8.10^3 per well in a µClear 96-well plate (Greiner Bio-One) as previously described[49]. SARS-CoV-2 and VOC viruses (multiplicity of infection, 0.1) were incubated with recombinant IgG1, at 1µg/ml for non-Omicron variants and 10µg/ml for omicron variants. Titration was performed from 9µg/ml with 11 consecutive 1:4 dilutions for the 6 most potent antibodies. Culture medium were added for 30 min at room temperature to S-Fuse cells. The cells were fixed 18 h later in 2% paraformaldehyde, washed, and stained with Hoechst stain (dilution 1:1,000; Invitrogen). Images were acquired with an Opera Phenix high-content confocal microscope (Perkin-Elmer). The area displaying GFP expression, and the number of nuclei were quantified with Harmony software 4.8 (Perkin-Elmer). The percentage neutralization was calculated from the GFP-positive area as follows: 100 × [1 − (value with IgA/IgG− value in “non-infected”)/(value in “no IgA/IgG” − value in “non-infected”)]. IC50 values were calculated using Prism software (v.9.3.1; GraphPad Prism Inc.) by fitting replicate values using the four-parameter dose–response model (variable slope).

Pseudo-neutralization assay
Recombinant monoclonal antibodies have been tested using SARS-CoV-2 HiBiT-PsVLP Assay (Promega) following manufacturer’s instructions. Briefly, antibody-VLPs were incubated together 30min at 37°C. Antibody-VLP complexes were then added to extemporaneously thawed HEK293T LgBit cells along with DrkBit Peptide during 3h incubation. Nano-Glo Live Cell reagents was then added to the cells for a 15-minute incubation. Bioluminescence was measured with SAFAS Xenius (SAFAS Monaco) plate reader. Antibodies have been tested at 1µg/ml with D614G HiBiT-PsVLPs and 10µg/ml with BA.1 and BA.5 HiBiT-PsVLPs. The percentage inhibition was calculated from bioluminescent signal by substracting the mock and as follows : 100 × [1 − (mAb bioluminescence signal/no mAb bioluminescence signal)].

ADCP assay
PBMCs were isolated from healthy donors' blood (Etablissement Français du Sang) using Ficoll Plaque Plus (GE Healthcare). Primary human monocytes were purified from PBMCs by magnetic-sorted cell sorting using Whole Blood CD14 MicroBeads (Miltenyi Biotech).
Biotinylated-SARS-CoV-2 tri-S proteins were incubated with FITC-labeled NeutrAvidin beads (1 µm; Thermo Fisher Scientific; 20 µg of tri-S for 2 µl of beads), washed, and incubated for 30 min at room temperature. After PBS washings, tri-S Wuhan coupled-beads 1:10000-diluted in DMEM were incubated for 1 h at 37°C with 4.5µL of human IgG1 antibodies (at 5 µg/ml). The tri-S-bead-antibody mixtures were then incubated with 1.10^5 human monocytes for 2 h at 37°C. Following washings with PBS, cells were fixed with 4% PFA–PBS and analyzed using a CytoFLEX flow cytometer (Beckman Coulter). ADCP assays were analyzed using the FlowJo software (v10.8; FlowJo LLC). ADCP score was established by measuring the percentage of FITC positive cells.

ADCC assay
The ADCC activity of anti–SARS-CoV-2 tri-S IgG antibodies were determined using the ADCC Reporter Bioassay following manufacturer's instructions (Promega). Briefly, 1. 10^5 tri-S Wuhan-transfected HEK293F cells were co-cultured with 6.10^4 Jurkat-CD16-NFATrLuc cells in the presence or absence of SARS-CoV-2 RBD–specific or control mGO53 IgG antibody at 10 µg/ml. Luciferase was measured after 16 h of incubation using an GloMax Discoverer® plate reader (Promega). ADCC score was measured as the fold induction of luciferase activity vs. without antibody.

CD assay
The complement deposition of RBD–specific antibodies was measured by evaluating SARS-CoV-2 S Wuhan–expressing HEK293F cells as previously described[21]. Briefly, 2.10^5 HEK293F - Spike cells were cultivated in the presence of 50% normal or heat-inactivated human serum, and with or without IgG antibodies at 10 µg/ml. After 24 h, the cells were washed with PBS and incubated for 30 min at 4°C with the live/dead fixable aqua dead cell marker (1:1,000 in PBS; Life Technologies). Concomitantly, CD readout was measured with complement deposition in flow cytometry adding mouse anti-human antibody C3/C3b/iC3b-PE (6C9; BD Pharmingen) at 2µg/ml. Data were acquired on Cytoflex (Beckman Coulter). CD score was calculated using the gMFI of live cells with mAb and normal serum divided by the gMFI of live cells without mAb.

Bioinformatics & statistics
Statistical analyses and most of the graphical representation were performed using GraphPad Prism software (v.8.2; GraphPad Prism Inc.). Representations were refined using Adobe Illustrator (v26.2; Adobe Inc.). The numbers of V , Vκ, and Vλ mutations were compared across groups of antibodies using unpaired Student's t test. mAb class statistical comparison for functional tests and neutralization assays were performed with Mann-Whitney's. Volcano plot gene feature statistical comparison (n = 206 parameters) was done by Fischer's exact test. Dual RBD/tri-S baiting was compared by Fischer's exact test. Heatmap representation was performed using Prism or complex heatmap R package (v2.10.0; https://www.bioconductor.org/packages/release/bioc/html/ComplexHeatmap.html). PCA plots were generated using the factoextra package (v1.0.7; https://CRAN.Rproject.org/package=factoextra). Synergy representation were perfomed by Synergy finder tool using ZIP method (v3.0; https://synergyfinder.fimm.fi/synergy/20231211114812308925/).

References

1. Barouch, D.H. (2022). Covid-19 Vaccines — Immunity, Variants, Boosters. N. Engl. J. Med. *387*, 1011–1020. https://doi.org/10.1056/nejmra2206573.
2. Qi, H., Liu, B., Wang, X., and Zhang, L. (2022). The humoral response and antibodies against SARS-CoV-2 infection. Nat. Immunol. *23*, 1008–1020. https://doi.org/10.1038/s41590-022-01248-5.
3. Röltgen, K., and Boyd, S.D. (2024). Antibody and B Cell Responses to SARS-CoV-2 Infection and Vaccination: The End of the Beginning. Annu. Rev. Pathol. Mech. Dis. *19*, 69–97. https://doi.org/10.1146/annurev-pathmechdis-031521-042754.
4. Piccoli, L., Park, Y.J., Tortorici, M.A., Czudnochowski, N., Walls, A.C., Beltramello, M., Silacci-Fregni, C., Pinto, D., Rosen, L.E., Bowen, J.E., et al. (2020). Mapping Neutralizing and Immunodominant Sites on the SARS-CoV-2 Spike Receptor-Binding Domain by Structure-Guided High-Resolution Serology. Cell *183*, 1024-1042.e21. https://doi.org/10.1016/j.cell.2020.09.037.
5. Rouet, R., Henry, J.Y., Johansen, M.D., Sobti, M., Balachandran, H., Langley, D.B., Walker, G.J., Lenthall, H., Jackson, J., Ubiparipovic, S., et al. (2023). Broadly neutralizing SARS-CoV-2 antibodies through epitope-based selection from convalescent patients. Nat. Commun. *14*, 687. https://doi.org/10.1038/s41467-023-36295-5.
6. Barnes, C.O., Jette, C.A., Abernathy, M.E., Dam, K.-M.A., Esswein, S.R., Gristick, H.B., Malyutin, A.G., Sharaf, N.G., Huey-Tubman, K.E., Lee, Y.E., et al. (2020). SARS-CoV-2 neutralizing antibody structures inform therapeutic strategies. Nature *588*, 682–687. https://doi.org/10.1038/s41586-020-2852-1.
7. Chen, Y., Zhao, X., Zhou, H., Zhu, H., Jiang, S., and Wang, P. (2022). Broadly neutralizing antibodies to SARS-CoV-2 and other human coronaviruses. Nat. Rev. Immunol. *4*. https://doi.org/10.1038/s41577-022-00784-3.
8. Corti, D., Purcell, L.A., Snell, G., and Veesler, D. (2021). Tackling COVID-19 with neutralizing monoclonal antibodies. Cell *184*, 3086–3108. https://doi.org/10.1016/j.cell.2021.05.005.
9. Gruell, H., Vanshylla, K., Weber, T., Barnes, C.O., Kreer, C., and Klein, F. (2022). Antibody-mediated neutralization of SARS-CoV-2. Immunity *55*, 925–944. https://doi.org/10.1016/j.immuni.2022.05.005.
10. Carabelli, A.M., Peacock, T.P., Thorne, L.G., Harvey, W.T., Hughes, J., de Silva, T.I., Peacock, S.J., Barclay, W.S., de Silva, T.I., Towers, G.J., et al. (2023). SARS-CoV-2 variant biology: immune escape, transmission and fitness. Nat. Rev. Microbiol. *21*, 162–177. https://doi.org/10.1038/s41579-022-00841-7.
11. Roemer, C., Sheward, D.J., Hisner, R., Gueli, F., Sakaguchi, H., Frohberg, N., Schoenmakers, J., Sato, K., O'Toole, Á., Rambaut, A., et al. (2023). SARS-CoV-2 evolution in the Omicron era. Nat. Microbiol. *8*, 1952–1959. https://doi.org/10.1038/s41564-023-01504-w.
12. Wang, Q., Iketani, S., Li, Z., Liu, L., Guo, Y., Huang, Y., Bowen, A.D., Liu, M., Wang, M., Yu, J., et al. (2022). Alarming antibody evasion properties of rising SARS-CoV-2 BQ and XBB subvariants. Cell. https://doi.org/10.1016/j.cell.2022.12.018.
13. Westendorf, K., Žentelis, S., Wang, L., Foster, D., Vaillancourt, P., Wiggin, M., Lovett, E., van der Lee, R., Hendle, J., Pustilnik, A., et al. (2022). LY-CoV1404 (bebtelovimab) potently neutralizes SARS-CoV-2 variants. Cell Rep. *39*. https://doi.org/10.1016/j.celrep.2022.110812.
14. Taylor, P.C., Adams, A.C., Hufford, M.M., de la Torre, I., Winthrop, K., and Gottlieb, R.L. (2021). Neutralizing monoclonal antibodies for treatment of COVID-19. Nat. Rev. Immunol. *21*, 382–393. https://doi.org/10.1038/s41577-021-00542-x.
15. Li, G., Hilgenfeld, R., Whitley, R., and De Clercq, E. (2023). Therapeutic strategies for COVID-19: progress and lessons learned. Nat. Rev. Drug Discov. *22*, 449–475. https://doi.org/10.1038/s41573-023-00672-y.
16. Gliga, S., Lübke, N., Killer, A., Gruell, H., Walker, A., Dilthey, A.T., Thielen, A., Lohr,

C., Flaßhove, C., Krieg, S., et al. (2022). Rapid Selection of Sotrovimab Escape Variants in Severe Acute Respiratory Syndrome Coronavirus 2 (SARS-CoV-2) Omicron-Infected Immunocompromised Patients. Clin. Infect. Dis., 5–6. https://doi.org/10.1093/cid/ciac802.

17. Planas, D., Bruel, T., Staropoli, I., Guivel-Benhassine, F., Porrot, F., Maes, P., Grzelak, L., Prot, M., Mougari, S., Planchais, C., et al. (2023). Resistance of Omicron subvariants BA.2.75.2, BA.4.6, and BQ.1.1 to neutralizing antibodies. Nat. Commun. *14*, 1–11. https://doi.org/10.1038/s41467-023-36561-6.
18. Cao, Y., Jian, F., Zhang, Z., Yisimayi, A., Hao, X., Bao, L., Yuan, F., Yu, Y., Du, S., Wang, J., et al. (2022). Rational identification of potent and broad sarbecovirus-neutralizing antibody cocktails from SARS convalescents. Cell Rep. *41*, 111845. https://doi.org/10.1016/j.celrep.2022.111845.
19. Rosen, L.E., Tortorici, M.A., De Marco, A., Pinto, D., Foreman, W.B., Taylor, A.L., Park, Y.J., Bohan, D., Rietz, T., Errico, J.M., et al. (2024). A potent pan-sarbecovirus neutralizing antibody resilient to epitope diversification. Cell, 1–18. https://doi.org/10.1016/j.cell.2024.09.026.
20. Ellis, R., and Weiss, A. (2025). Human vaccines and immunotherapeutics: News February 2025. Hum. Vaccines Immunother. *21*, 4–5. https://doi.org/10.1080/21645515.2025.2482479.
21. Dufloo, J., Grzelak, L., Staropoli, I., Madec, Y., Tondeur, L., Anna, F., Pelleau, S., Wiedemann, A., Planchais, C., Buchrieser, J., et al. (2021). Asymptomatic and symptomatic SARS-CoV-2 infections elicit polyfunctional antibodies. Cell Reports Med. *2*. https://doi.org/10.1016/j.xcrm.2021.100275.
22. Planchais, C., Fernández, I., Bruel, T., de Melo, G.D., Prot, M., Beretta, M., Guardado-Calvo, P., Dufloo, J., Molinos-Albert, L.M., Backovic, M., et al. (2022). Potent human broadly SARS-CoV-2–neutralizing IgA and IgG antibodies effective against Omicron BA.1 and BA.2. J. Exp. Med. *219*. https://doi.org/10.1084/jem.20220638.
23. Schäfer, A., Muecksch, F., Lorenzi, J.C.C., Leist, S.R., Cipolla, M., Bournazos, S., Schmidt, F., Maison, R.M., Gazumyan, A., Martinez, D.R., et al. (2020). Antibody potency, effector function, and combinations in protection and therapy for SARS-cov-2 infection in vivo. J. Exp. Med. *218*. https://doi.org/10.1084/JEM.20201993.
24. Anand, S.P., Prévost, J., Nayrac, M., Beaudoin-Bussières, G., Benlarbi, M., Gasser, R., Brassard, N., Laumaea, A., Gong, S.Y., Bourassa, C., et al. (2021). Longitudinal analysis of humoral immunity against SARS-CoV-2 Spike in convalescent individuals up to 8 months post-symptom onset. Cell Reports Med. *2*. https://doi.org/10.1016/j.xcrm.2021.100290.
25. Zohar, T., Loos, C., Fischinger, S., Atyeo, C., Wang, C., Slein, M.D., Burke, J., Yu, J., Feldman, J., Hauser, B.M., et al. (2020). Compromised Humoral Functional Evolution Tracks with SARS-CoV-2 Mortality. Cell *183*, 1508-1519.e12. https://doi.org/10.1016/j.cell.2020.10.052.
26. Izadi, A., and Nordenfelt, P. (2024). Protective non-neutralizing SARS-CoV-2 monoclonal antibodies. Trends Immunol. *xx*, 1–16. https://doi.org/10.1016/j.it.2024.06.003.
27. Kaplonek, P., Cizmeci, D., Fischinger, S., Collier, A.R., Suscovich, T., Linde, C., Broge, T., Mann, C., Amanat, F., Dayal, D., et al. (2022). mRNA-1273 and BNT162b2 COVID-19 vaccines elicit antibodies with differences in Fc-mediated effector functions. Sci. Transl. Med. *14*, 1–12. https://doi.org/10.1126/scitranslmed.abm2311.
28. Hederman, A.P., Natarajan, H., Heyndrickx, L., Ariën, K.K., Wiener, J.A., Wright, P.F., Bloch, E.M., Tobian, A.A.R., Redd, A.D., Blankson, J.N., et al. (2023). SARS-CoV-2 vaccination elicits broad and potent antibody effector functions to variants of concern in vulnerable populations. Nat. Commun. *14*, 1–11. https://doi.org/10.1038/s41467-023-40960-0.
29. Ullah, I., Beaudoin-Bussières, G., Symmes, K., Cloutier, M., Ducas, E., Tauzin, A., Laumaea, A., Grunst, M.W., Dionne, K., Richard, J., et al. (2023). The Fc-effector function of COVID-19 convalescent plasma contributes to SARS-CoV-2 treatment

efficacy in mice. Cell Reports Med. *4*. https://doi.org/10.1016/j.xcrm.2022.100893.
30. Clark, J., Hoxie, I., Adelsberg, D.C., Sapse, I.A., Andreata-Santos, R., Yong, J.S., Amanat, F., Tcheou, J., Raskin, A., Singh, G., et al. (2024). Protective effect and molecular mechanisms of human non-neutralizing cross-reactive spike antibodies elicited by SARS-CoV-2 mRNA vaccination. bioRxiv Prepr. Serv. Biol. https://doi.org/10.1016/j.celrep.2024.114922.
31. Bruel, T., Vrignaud, L.-L., Porrot, F., Staropoli, I., Planas, D., Guivel-Benhassine, F., Puech, J., Prot, M., Munier, S., Henry-Bolland, W., et al. (2023). Antiviral activities of sotrovimab against BQ.1.1 and XBB.1.5 in sera of treated patients, https://doi.org/10.1101/2023.05.25.23290512 https://doi.org/10.1101/2023.05.25.23290512.
32. Addetia, A., Crawford, K.H.D., Dingens, A., Zhu, H., Roychoudhury, P., Huang, M.-L., Jerome, K.R., Bloom, J.D., and Greninger, A.L. (2020). Neutralizing Antibodies Correlate with Protection from SARS-CoV-2 in Humans during a Fishery Vessel Outbreak with a High Attack Rate. J. Clin. Microbiol. *58*, 1–32. https://doi.org/10.1128/JCM.02107-20.
33. Low, J.S., Jerak, J., Tortorici, M.A., McCallum, M., Pinto, D., Cassotta, A., Foglierini, M., Mele, F., Abdelnabi, R., Weynand, B., et al. (2022). ACE2-binding exposes the SARS-CoV-2 fusion peptide to broadly neutralizing coronavirus antibodies. Science (80-.). *377*, 735–742. https://doi.org/10.1126/science.abq2679.
34. Bianchini, F., Crivelli, V., Abernathy, M.E., Guerra, C., Palus, M., Muri, J., Marcotte, H., Piralla, A., Pedotti, M., De Gasparo, R., et al. (2023). Human neutralizing antibodies to cold linear epitopes and subdomain 1 of the SARS-CoV-2 spike glycoprotein. Sci. Immunol. *8*, 1–18. https://doi.org/10.1126/sciimmunol.ade0958.
35. Sun, X., Yi, C., Zhu, Y., Ding, L., Xia, S., Chen, X., Liu, M., Gu, C., Lu, X., Fu, Y., et al. (2022). Neutralization mechanism of a human antibody with pan-coronavirus reactivity including SARS-CoV-2. Nat. Microbiol. *7*, 1063–1074. https://doi.org/10.1038/s41564-022-01155-3.
36. Prigent, J., Lorin, V., Kök, A., Hieu, T., Bourgeau, S., and Mouquet, H. (2016). Scarcity of autoreactive human blood IgA+ memory B cells. Eur. J. Immunol. *46*, 2340–2351. https://doi.org/10.1002/eji.201646446.
37. Seydoux, E., Homad, L.J., MacCamy, A.J., Parks, K.R., Hurlburt, N.K., Jennewein, M.F., Akins, N.R., Stuart, A.B., Wan, Y.-H.H., Feng, J., et al. (2020). Analysis of a SARS-CoV-2-Infected Individual Reveals Development of Potent Neutralizing Antibodies with Limited Somatic Mutation. Immunity *53*, 98-105.e5. https://doi.org/10.1016/j.immuni.2020.06.001.
38. Barnes, C.O., West, A.P., Huey-Tubman, K.E., Hoffmann, M.A.G., Sharaf, N.G., Hoffman, P.R., Koranda, N., Gristick, H.B., Gaebler, C., Muecksch, F., et al. (2020). Structures of Human Antibodies Bound to SARS-CoV-2 Spike Reveal Common Epitopes and Recurrent Features of Antibodies. Cell *182*, 828-842.e16. https://doi.org/10.1016/j.cell.2020.06.025.
39. Planchais, C., Fernández, I., Bruel, T., Dias De Melo, G., Prot, M., Beretta, M., Guardado-Calvo, P., Dufloo, J., Molinos-Albert, L.M., Backovic, M., et al. Potent Human Broadly SARS-CoV-2 Neutralizing IgA and IgG Antibodies Effective Against Omicron BA.1 and BA.2. https://doi.org/10.1101/2022.04.01.486719.
40. Greaney, A.J., Starr, T.N., Barnes, C.O., Weisblum, Y., Schmidt, F., Caskey, M., Gaebler, C., Cho, A., Agudelo, M., Finkin, S., et al. (2021). Mapping mutations to the SARS-CoV-2 RBD that escape binding by different classes of antibodies. Nat. Commun. *12*. https://doi.org/10.1038/s41467-021-24435-8.
41. Carabelli, A.M., Peacock, T.P., Thorne, L.G., Harvey, W.T., Hughes, J., de Silva, T.I., Peacock, S.J., Barclay, W.S., de Silva, T.I., Towers, G.J., et al. (2023). SARS-CoV-2 variant biology: immune escape, transmission and fitness. Nat. Rev. Microbiol. https://doi.org/10.1038/s41579-022-00841-7.
42. Hansen, J., Baum, A., Pascal, K.E., Russo, V., Giordano, S., Wloga, E., Fulton, B.O., Yan, Y., Koon, K., Patel, K., et al. (2020). Studies in humanized mice and

convalescent humans yield a SARS-CoV-2 antibody cocktail. Science (80-.). *369*, 1010–1014. https://doi.org/10.1126/science.abd0827.
43. Shi, Y., Wang, Y., Shao, C., Huang, J., Gan, J., Huang, X., Bucci, E., Piacentini, M., Ippolito, G., and Melino, G. (2020). COVID-19 infection: the perspectives on immune responses. Cell Death Differ. *27*, 1451–1454. https://doi.org/10.1038/s41418-020-0530-3.
44. Jones, B.E., Brown-Augsburger, P.L., Corbett, K.S., Westendorf, K., Davies, J., Cujec, T.P., Wiethoff, C.M., Blackbourne, J.L., Heinz, B.A., Foster, D., et al. (2021). The neutralizing antibody, LY-CoV555, protects against SARS-CoV-2 infection in nonhuman primates. Sci. Transl. Med. *13*, 1–18. https://doi.org/10.1126/scitranslmed.abf1906.
45. Kim, C., Ryu, D.K., Lee, J., Kim, Y. Il, Seo, J.M., Kim, Y.G., Jeong, J.H., Kim, M., Kim, J.I., Kim, P., et al. (2021). A therapeutic neutralizing antibody targeting receptor binding domain of SARS-CoV-2 spike protein. Nat. Commun. *12*, 1–10. https://doi.org/10.1038/s41467-020-20602-5.
46. Zost, S.J., Gilchuk, P., Case, J.B., Binshtein, E., Chen, R.E., Nkolola, J.P., Schäfer, A., Reidy, J.X., Trivette, A., Nargi, R.S., et al. (2020). Potently neutralizing and protective human antibodies against SARS-CoV-2. Nature *584*, 443–449. https://doi.org/10.1038/s41586-020-2548-6.
47. Garrett Rappazzo, C., Tse, L. V., Kaku, C.I., Wrapp, D., Sakharkar, M., Huang, D., Deveau, L.M., Yockachonis, T.J., Herbert, A.S., Battles, M.B., et al. (2021). Broad and potent activity against SARS-like viruses by an engineered human monoclonal antibody. Science (80-.). *371*, 823–829. https://doi.org/10.1126/science.abf4830.
48. Pinto, D., Park, Y.J., Beltramello, M., Walls, A.C., Tortorici, M.A., Bianchi, S., Jaconi, S., Culap, K., Zatta, F., De Marco, A., et al. (2020). Cross-neutralization of SARS-CoV-2 by a human monoclonal SARS-CoV antibody. Nature *583*, 290–295. https://doi.org/10.1038/s41586-020-2349-y.
49. Buchrieser, J., Dufloo, J., Hubert, M., Monel, B., Planas, D., Rajah, M.M., Planchais, C., Porrot, F., Guivel-Benhassine, F., Van der Werf, S., et al. (2020). Syncytia formation by SARS-CoV-2-infected cells. EMBO J. *39*, 1–12. https://doi.org/10.15252/embj.2020106267.
50. Duan, X., Shi, R., Liu, P., Huang, Q., Wang, F., Chen, X., Feng, H., Huang, W., Xiao, J., and Yan, J. (2022). A non-ACE2-blocking neutralizing antibody against Omicron-included SARS-CoV-2 variants. Signal Transduct. Target. Ther. *7*, 2021–2023. https://doi.org/10.1038/s41392-022-00879-2.
51. Jangra, S., Ye, C., Rathnasinghe, R., Stadlbauer, D., Krammer, F., Simon, V., Martinez-Sobrido, L., García-Sastre, A., Schotsaert, M., Alshammary, H., et al. (2021). SARS-CoV-2 spike E484K mutation reduces antibody neutralisation. The Lancet Microbe *2*, e283–e284. https://doi.org/10.1016/S2666-5247(21)00068-9.
52. Dacon, C., Tucker, C., Peng, L., Lee, C.C.D., Lin, T.H., Yuan, M., Cong, Y., Wang, L., Purser, L., Williams, J.K., et al. (2022). Broadly neutralizing antibodies target the coronavirus fusion peptide. Science (80-.). *377*, 728–735. https://doi.org/10.1126/science.abq3773.
53. Shi, R., Shan, C., Duan, X., Chen, Z., Liu, P., Song, J., Song, T., Bi, X., Han, C., Wu, L., et al. (2020). A human neutralizing antibody targets the receptor-binding site of SARS-CoV-2. Nature *584*, 120–124. https://doi.org/10.1038/s41586-020-2381-y.
54. Cox, M.G., Peacock, T.P., Harvey, W.T., Hughes, J., Wright, D.W., Willett, B.J., Thomson, E., Gupta, R.K., Peacock, S.J., Robertson, D.L., et al. (2023). SARS-CoV-2 variant evasion of monoclonal antibodies based on in vitro studies. Nat. Rev. Microbiol. *21*, 112–124. https://doi.org/10.1038/s41579-022-00809-7.
55. Cao, Y., Yisimayi, A., Jian, F., Song, W., Xiao, T., Wang, L., Du, S., Wang, J., Li, Q., Chen, X., et al. (2022). BA.2.12.1, BA.4 and BA.5 escape antibodies elicited by Omicron infection. Nature *608*, 593–602. https://doi.org/10.1038/s41586-022-04980-y.
56. Gruell, H., Vanshylla, K., Korenkov, M., Tober-Lau, P., Zehner, M., Münn, F., Janicki, H., Augustin, M., Schommers, P., Sander, L.E., et al. (2022). SARS-CoV-2 Omicron

sublineages exhibit distinct antibody escape patterns. Cell Host Microbe *30*, 1231-1241.e6. https://doi.org/10.1016/j.chom.2022.07.002.
57. Johnson, N. V., Wall, S.C., Kramer, K.J., Holt, C.M., Periasamy, S., Richardson, S.I., Manamela, N.P., Suryadevara, N., Andreano, E., Paciello, I., et al. (2024). Discovery and characterization of a pan-betacoronavirus S2-binding antibody. Structure *32*, 1893-1909.e11. https://doi.org/10.1016/j.str.2024.08.022.
58. Harris, C., Kapingidza, A.B., San, J.E., Christopher, J., Gavitt, T., Rhodes, B., Janowska, K., O'Donnell, C., Lindenberger, J., Huang, X., et al. (2025). Design of SARS-CoV-2 RBD Immunogens to Focus Immune Responses Towards Conserved Coronavirus Epitopes, https://doi.org/10.1101/2025.01.09.632180 https://doi.org/10.1101/2025.01.09.632180.
59. Tan, T.J.C., Verma, A.K., Odle, A., Lei, R., Meyerholz, D.K., Matreyek, K.A., Perlman, S., Wong, L.-Y.R., and Wu, N.C. (2024). Evidence of antigenic drift in the fusion machinery core of SARS-CoV-2 spike. Proc. Natl. Acad. Sci. *121*, 2017. https://doi.org/10.1073/pnas.2317222121.
60. Yuan, M., and Wilson, I.A. (2024). Structural Immunology of SARS-CoV-2. Immunol. Rev., 1–25. https://doi.org/10.1111/imr.13431.
61. Takeshita, M., Fukuyama, H., Kamada, K., Matsumoto, T., Makino-Okamura, C., Lin, Q., Sakuma, M., Kawahara, E., Yamazaki, I., Uchikubo-Kamo, T., et al. (2023). Potent neutralizing broad-spectrum antibody against SARS-CoV-2 generated from dual-antigen-specific B cells from convalescents. iScience *26*. https://doi.org/10.1016/j.isci.2023.106955.
62. Winkler, E.S., Gilchuk, P., Yu, J., Bailey, A.L., Chen, R.E., Chong, Z., Zost, S.J., Jang, H., Huang, Y., Allen, J.D., et al. (2021). Human neutralizing antibodies against SARS-CoV-2 require intact Fc effector functions for optimal therapeutic protection. Cell *184*, 1804-1820.e16. https://doi.org/10.1016/j.cell.2021.02.026.
63. Wines, B.D., Kurtovic, L., Trist, H.M., Esparon, S., Lopez, E., Chappin, K., Chan, L.J., Mordant, F.L., Lee, W.S., Gherardin, N.A., et al. (2022). Fc engineered ACE2-Fc is a potent multifunctional agent targeting SARS-CoV2. Front. Immunol. *13*, 1–15. https://doi.org/10.3389/fimmu.2022.889372.
64. Pierre, C.N., Adams, L.E., Anasti, K., Goodman, D., Stanfield-Oakley, S., Powers, J.M., Li, D., Rountree, W., Wang, Y., Edwards, R.J., et al. (2023). Non-neutralizing SARS-CoV-2 N-terminal domain antibodies protect mice against severe disease using Fc-mediated effector functions. bioRxiv, 2023.07.25.550460. https://doi.org/10.1101/2023.07.25.550460.
65. Java, A., Apicelli, A.J., Kathryn Liszewski, M., Coler-Reilly, A., Atkinson, J.P., Kim, A.H.J., and Kulkarni, H.S. (2020). The complement system in COVID-19: Friend and foe? JCI Insight *5*, 1–12. https://doi.org/10.1172/jci.insight.140711.
66. Zhang, A., Stacey, H.D., D'Agostino, M.R., Tugg, Y., Marzok, A., and Miller, M.S. (2023). Beyond neutralization: Fc-dependent antibody effector functions in SARS-CoV-2 infection. Nat. Rev. Immunol. *23*, 381–396. https://doi.org/10.1038/s41577-022-00813-1.
67. Zhou, X., Ma, F., Xie, J., Yuan, M., Li, Y., Shaabani, N., Zhao, F., Huang, D., Wu, N.C., Lee, C.C.D., et al. (2021). Diverse immunoglobulin gene usage and convergent epitope targeting in neutralizing antibody responses to SARS-CoV-2. Cell Rep. *35*, 109109. https://doi.org/10.1016/j.celrep.2021.109109.
68. Carvelli, J., Demaria, O., Vély, F., Batista, L., Chouaki Benmansour, N., Fares, J., Carpentier, S., Thibult, M.L., Morel, A., Remark, R., et al. (2020). Association of COVID-19 inflammation with activation of the C5a–C5aR1 axis. Nature *588*, 146–150. https://doi.org/10.1038/s41586-020-2600-6.
69. Gralinski, L.E., Sheahan, T.P., Morrison, T.E., Menachery, V.D., Jensen, K., Leist, S.R., Whitmore, A., Heise, M.T., and Baric, R.S. (2018). Complement activation contributes to severe acute respiratory syndrome coronavirus pathogenesis. MBio *9*. https://doi.org/10.1128/mBio.01753-18.
70. Tauzin, A., Nayrac, M., Benlarbi, M., Gong, S.Y., Gasser, R., Beaudoin-Bussières, G.,

Brassard, N., Laumaea, A., Vézina, D., Prévost, J., et al. (2021). A single dose of the SARS-CoV-2 vaccine BNT162b2 elicits Fc-mediated antibody effector functions and T cell responses. Cell Host Microbe *29*, 1137-1150.e6. https://doi.org/10.1016/j.chom.2021.06.001.

71. Yu, Y., Wang, M., Zhang, X., Li, S., Lu, Q., Zeng, H., Hou, H., Li, H., Zhang, M., Jiang, F., et al. (2021). Antibody-dependent cellular cytotoxicity response to SARS-CoV-2 in COVID-19 patients. Signal Transduct. Target. Ther. *6*. https://doi.org/10.1038/s41392-021-00759-1.
72. Lee, W.S., Selva, K.J., Davis, S.K., Wines, B.D., Reynaldi, A., Esterbauer, R., Kelly, H.G., Haycroft, E.R., Tan, H.X., Juno, J.A., et al. (2021). Decay of Fc-dependent antibody functions after mild to moderate COVID-19. Cell Reports Med. *2*, 100296. https://doi.org/10.1016/j.xcrm.2021.100296.
73. Julg, B., Stephenson, K.E., Wagh, K., Tan, S.C., Zash, R., Walsh, S., Ansel, J., Kanjilal, D., Nkolola, J., Walker-Sperling, V.E.K., et al. (2022). Safety and antiviral activity of triple combination broadly neutralizing monoclonal antibody therapy against HIV-1: a phase 1 clinical trial. Nat. Med. *28*, 1288–1296. https://doi.org/10.1038/s41591-022-01815-1.
74. Zhao, X., Howell, K.A., He, S., Brannan, J.M., Wec, A.Z., Davidson, E., Turner, H.L., Chiang, C.I., Lei, L., Fels, J.M., et al. (2017). Immunization-Elicited Broadly Protective Antibody Reveals Ebolavirus Fusion Loop as a Site of Vulnerability. Cell *169*, 891-904.e15. https://doi.org/10.1016/j.cell.2017.04.038.
75. Vigil, A., Frias-Staheli, N., Carabeo, T., and Wittekind, M. (2020). Airway Delivery of Anti-influenza Monoclonal Antibodies Results in Enhanced Antiviral Activities and Enables Broad-Coverage Combination Therapies. J. Virol. *94*, 1–20. https://doi.org/10.1128/jvi.00052-20.
76. Copin, R., Baum, A., Wloga, E., Pascal, K.E., Giordano, S., Fulton, B.O., Zhou, A., Negron, N., Lanza, K., Chan, N., et al. (2021). The monoclonal antibody combination REGEN-COV protects against SARS-CoV-2 mutational escape in preclinical and human studies. Cell *184*, 3949-3961.e11. https://doi.org/10.1016/j.cell.2021.06.002.
77. Mouquet, H. (2020). MARVellous Sidekick Antibodies. Cell Host Microbe *27*, 856–858. https://doi.org/10.1016/j.chom.2020.05.018.
78. Ilinykh, P.A., Huang, K., Santos, R.I., Gilchuk, P., Gunn, B.M., Karim, M.M., Liang, J., Fouch, M.E., Davidson, E., Parekh, D. V., et al. (2020). Non-neutralizing Antibodies from a Marburg Infection Survivor Mediate Protection by Fc-Effector Functions and by Enhancing Efficacy of Other Antibodies. Cell Host Microbe *27*, 976-991.e11. https://doi.org/10.1016/j.chom.2020.03.025.
79. Gilchuk, P., Murin, C.D., Milligan, J.C., Cross, R.W., Mire, C.E., Ilinykh, P.A., Huang, K., Kuzmina, N., Altman, P.X., Hui, S., et al. (2020). Analysis of a Therapeutic Antibody Cocktail Reveals Determinants for Cooperative and Broad Ebolavirus Neutralization. Immunity *52*, 388-403.e12. https://doi.org/10.1016/j.immuni.2020.01.001.
80. Cao, Y., Jian, F., Wang, J., Yu, Y., Song, W., Yisimayi, A., Wang, J., An, R., Chen, X., Zhang, N., et al. (2022). Imprinted SARS-CoV-2 humoral immunity induces convergent Omicron RBD evolution. Nature. https://doi.org/10.1038/s41586-022-05644-7.
81. Zhou, T., Wang, L., Misasi, J., Pegu, A., Zhang, Y., Harris, D.R., Olia, A.S., Talana, C.A., Yang, E.S., Chen, M., et al. (2022). Structural basis for potent antibody neutralization of SARS-CoV-2 variants including B.1.1.529. Science (80-.). https://doi.org/10.1126/science.abn8897.
82. Wang, P., Nair, M.S., Liu, L., Iketani, S., Luo, Y., Guo, Y., Wang, M., Yu, J., Zhang, B., Kwong, P.D., et al. (2021). Antibody resistance of SARS-CoV-2 variants B.1.351 and B.1.1.7. Nature *593*, 130–135. https://doi.org/10.1038/s41586-021-03398-2.
83. Wang, Q., Guo, Y., Iketani, S., Nair, M.S., Li, Z., Mohri, H., Wang, M., Yu, J., Bowen, A.D., Chang, J.Y., et al. (2022). Antibody evasion by SARS-CoV-2 Omicron subvariants BA.2.12.1, BA.4 and BA.5. Nature *608*, 603–608. https://doi.org/10.1038/s41586-022-05053-w.

84. Ai, J., Wang, X., He, X., Zhao, X., Zhang, Y., Jiang, Y., Li, M., Cui, Y., Chen, Y., Qiao, R., et al. (2022). Antibody evasion of SARS-CoV-2 Omicron BA.1, BA.1.1, BA.2, and BA.3 sub-lineages. Cell Host Microbe *30*, 1077-1083.e4. https://doi.org/10.1016/j.chom.2022.05.001.
85. Bruel, T., Hadjadj, J., Maes, P., Planas, D., Seve, A., Staropoli, I., Guivel-Benhassine, F., Porrot, F., Bolland, W.H., Nguyen, Y., et al. (2022). Serum neutralization of SARS-CoV-2 Omicron sublineages BA.1 and BA.2 in patients receiving monoclonal antibodies. Nat. Med. *28*, 1297–1302. https://doi.org/10.1038/s41591-022-01792-5.
86. Grzelak, L., Temmam, S., Planchais, C., Demeret, C., Tondeur, L., Huon, C., Guivel-Benhassine, F., Staropoli, I., Chazal, M., Dufloo, J., et al. (2020). A comparison of four serological assays for detecting anti–SARS-CoV-2 antibodies in human serum samples from different populations. Sci. Transl. Med. *12*, 1–13. https://doi.org/10.1126/SCITRANSLMED.ABC3103.
87. Planas, D., Bruel, T., Grzelak, L., Guivel-Benhassine, F., Staropoli, I., Porrot, F., Planchais, C., Buchrieser, J., Rajah, M.M., Bishop, E., et al. (2021). Sensitivity of infectious SARS-CoV-2 B.1.1.7 and B.1.351 variants to neutralizing antibodies. Nat. Med. *27*, 917–924. https://doi.org/10.1038/s41591-021-01318-5.
88. Planas, D., Veyer, D., Baidaliuk, A., Staropoli, I., Guivel-Benhassine, F., Rajah, M.M., Planchais, C., Porrot, F., Robillard, N., Puech, J., et al. (2021). Reduced sensitivity of SARS-CoV-2 variant Delta to antibody neutralization. Nature *596*, 276–280. https://doi.org/10.1038/s41586-021-03777-9.
89. Planas, D., Saunders, N., Maes, P., Guivel-Benhassine, F., Planchais, C., Buchrieser, J., Bolland, W.H., Porrot, F., Staropoli, I., Lemoine, F., et al. (2022). Considerable escape of SARS-CoV-2 Omicron to antibody neutralization. Nature *602*, 671–675. https://doi.org/10.1038/s41586-021-04389-z.
90. Betton, M., Livrozet, M., Planas, D., Fayol, A., Monel, B., Védie, B., Bruel, T., Tartour, E., Robillard, N., Manuguerra, J.C., et al. (2021). Sera Neutralizing Activities Against Severe Acute Respiratory Syndrome Coronavirus 2 and Multiple Variants 6 Months After Hospitalization for Coronavirus Disease 2019. Clin. Infect. Dis. *73*, E1337–E1344. https://doi.org/10.1093/cid/ciab308.
91. Lorin, V., and Mouquet, H. (2015). Efficient generation of human IgA monoclonal antibodies. J. Immunol. Methods *422*, 102–110. https://doi.org/10.1016/j.jim.2015.04.010.
92. Tiller, T., Meffre, E., Yurasov, S., Tsuiji, M., Nussenzweig, M.C., and Wardemann, H. (2008). Efficient generation of monoclonal antibodies from single human B cells by single cell RT-PCR and expression vector cloning. J. Immunol. Methods *329*, 112–124. https://doi.org/10.1016/j.jim.2007.09.017.
93. Mouquet, H., Klein, F., Scheid, J.F., Warncke, M., Pietzsch, J., Oliveira, T.Y.K., Velinzon, K., Seaman, M.S., and Nussenzweig, M.C. (2011). Memory B cell antibodies to HIV-1 gp140 cloned from individuals infected with clade A and B viruses. PLoS One *6*. https://doi.org/10.1371/journal.pone.0024078.
94. Mouquet, H., Scharf, L., Euler, Z., Liu, Y., Eden, C., Scheid, J.F., Halper-Stromberg, A., Gnanapragasam, P.N.P., Spencer, D.I.R., Seaman, M.S., et al. (2012). Complex-type N-glycan recognition by potent broadly neutralizing HIV antibodies. Proc. Natl. Acad. Sci. U. S. A. *109*. https://doi.org/10.1073/pnas.1217207109.
95. Planchais, C., Kök, A., Kanyavuz, A., Lorin, V., Bruel, T., Guivel-Benhassine, F., Rollenske, T., Prigent, J., Hieu, T., Prazuck, T., et al. (2019). HIV-1 Envelope Recognition by Polyreactive and Cross-Reactive Intestinal B Cells. Cell Rep. *27*, 572-585.e7. https://doi.org/10.1016/j.celrep.2019.03.032.
96. Wardemann, H., Yurasov, S., Schaefer, A., Young, J.W., Meffre, E., and Nussenzweig, M.C. (2003). Predominant autoantibody production by early human B cell precursors. Science (80-.). *301*, 1374–1377. https://doi.org/10.1126/science.1086907.
97. Meffre, E., Schaefer, A., Wardemann, H., Wilson, P., Davis, E., and Nussenzweig, M.C. (2004). Surrogate Light Chain Expressing Human Peripheral B Cells Produce

Self-reactive Antibodies. J. Exp. Med. *199*, 145–150. https://doi.org/10.1084/jem.20031550.

98. Planas, D., Staropoli, I., Michel, V., Lemoine, F., Donati, F., Prot, M., Porrot, F., Guivel-Benhassine, F., Jeyarajah, B., Brisebarre, A., et al. (2024). Distinct evolution of SARS-CoV-2 Omicron XBB and BA.2.86/JN.1 lineages combining increased fitness and antibody evasion. Nat. Commun. *15*. https://doi.org/10.1038/s41467-024-46490-7.

Figure 1

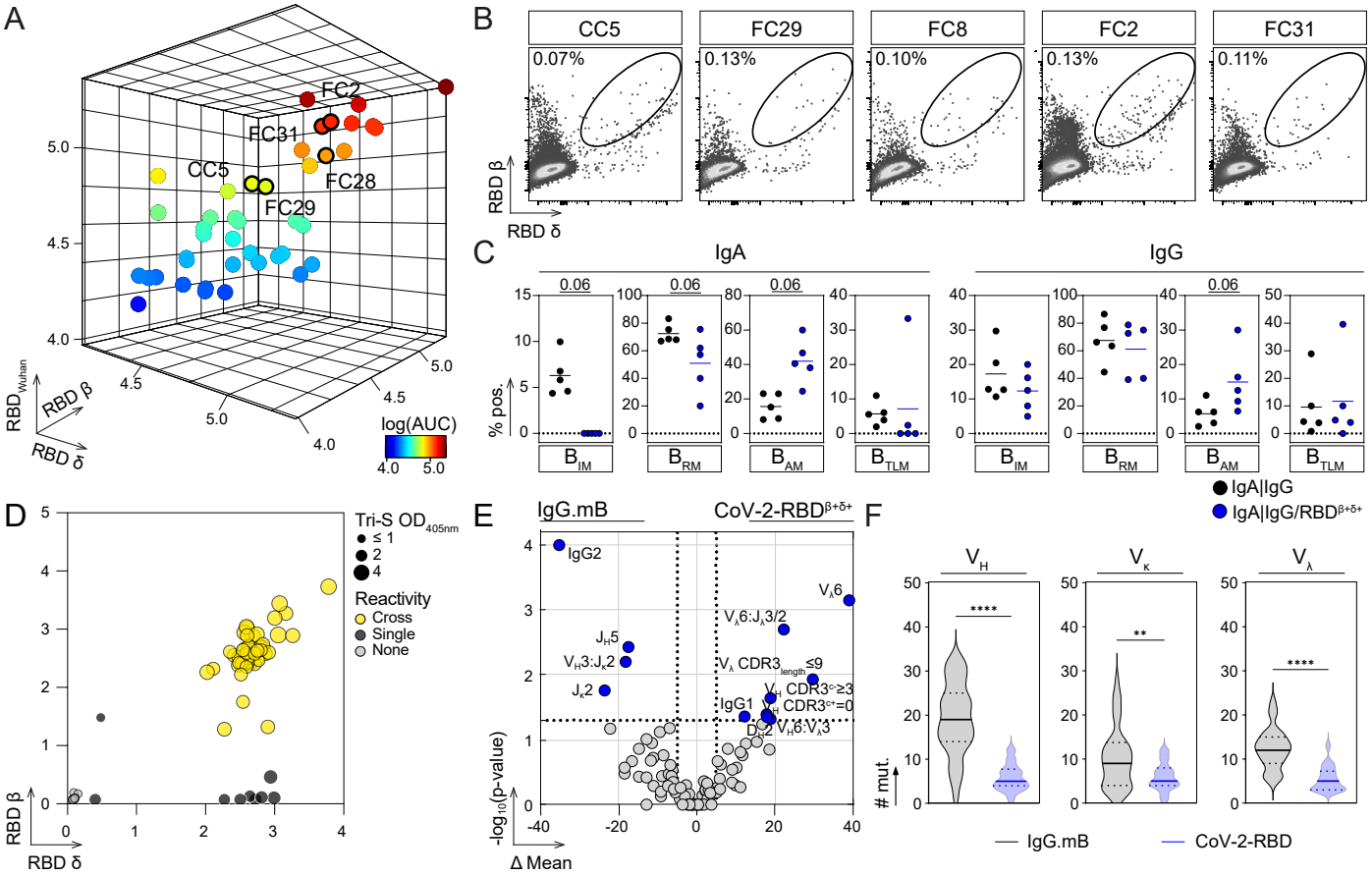
A
FC2
FC31
CC5
FC28
FC29
RBD β
RBD δ
log(AUC)
B
CC5
FC29
FC8
FC2
FC31
0.07%
0.13%
0.10%
0.13%
0.11%
RBD β
RBD δ
C
IgA
IgG
% pos.
IgA|IgG
IgA|IgG/RBD
D
Tri-S OD405nm
Reactivity
Cross
Single
None
RBD β
RBD δ
E
IgG.mB
CoV-2-RBD
IgG2
IgG1
-log10(p-value)
Δ Mean
F
mut.
IgG.mB
CoV-2-RBD

Figure 2

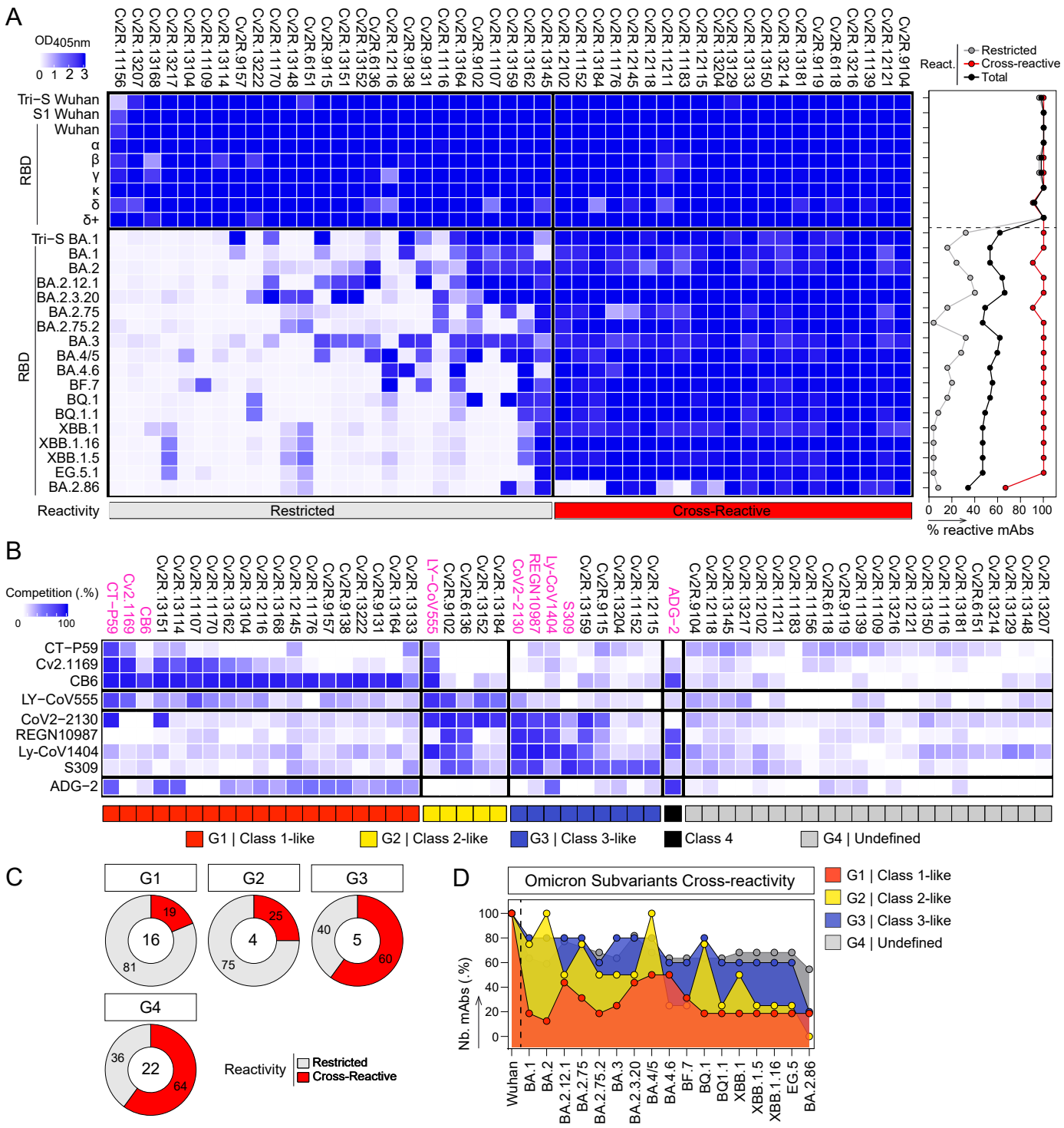
A
OD405nm
0 1 2 3
Tri-S Wuhan
S1 Wuhan
Wuhan
α
β
γ
κ
δ
δ+
RBD
Tri-S BA.1
BA.1
BA.2
BA.2.12.1
BA.2.3.20
BA.2.75
BA.2.75.2
BA.3
BA.4/5
BA.4.6
BF.7
BQ.1
BQ.1.1
XBB.1
XBB.1.16
XBB.1.5
EG.5.1
BA.2.86
Reactivity
Restricted
Cross-Reactive
React.
Restricted
Cross-reactive
Total
0 20 40 60 80 100
% reactive mAbs
B
Competition (.%)
0 100
CT-P59
Cv2.1169
CB6
LY-CoV555
CoV2-2130
REGN10987
Ly-CoV1404
S309
ADG-2
G1 | Class 1-like
G2 | Class 2-like
G3 | Class 3-like
Class 4
G4 | Undefined
C
G1
19
16
81
G2
25
4
75
G3
40
5
60
G4
36
22
64
Reactivity
Restricted
Cross-Reactive
D
Omicron Subvariants Cross-reactivity
Nb. mAbs (.%)
0 20 40 60 80 100
Wuhan
BA.1
BA.2
BA.2.12.1
BA.2.75
BA.2.75.2
BA.3
BA.2.3.20
BA.4/5
BA.4.6
BF.7
BQ.1
BQ.1.1
XBB.1
XBB.1.5
XBB.1.16
EG.5
BA.2.86
G1 | Class 1-like
G2 | Class 2-like
G3 | Class 3-like
G4 | Undefined

Figure 3

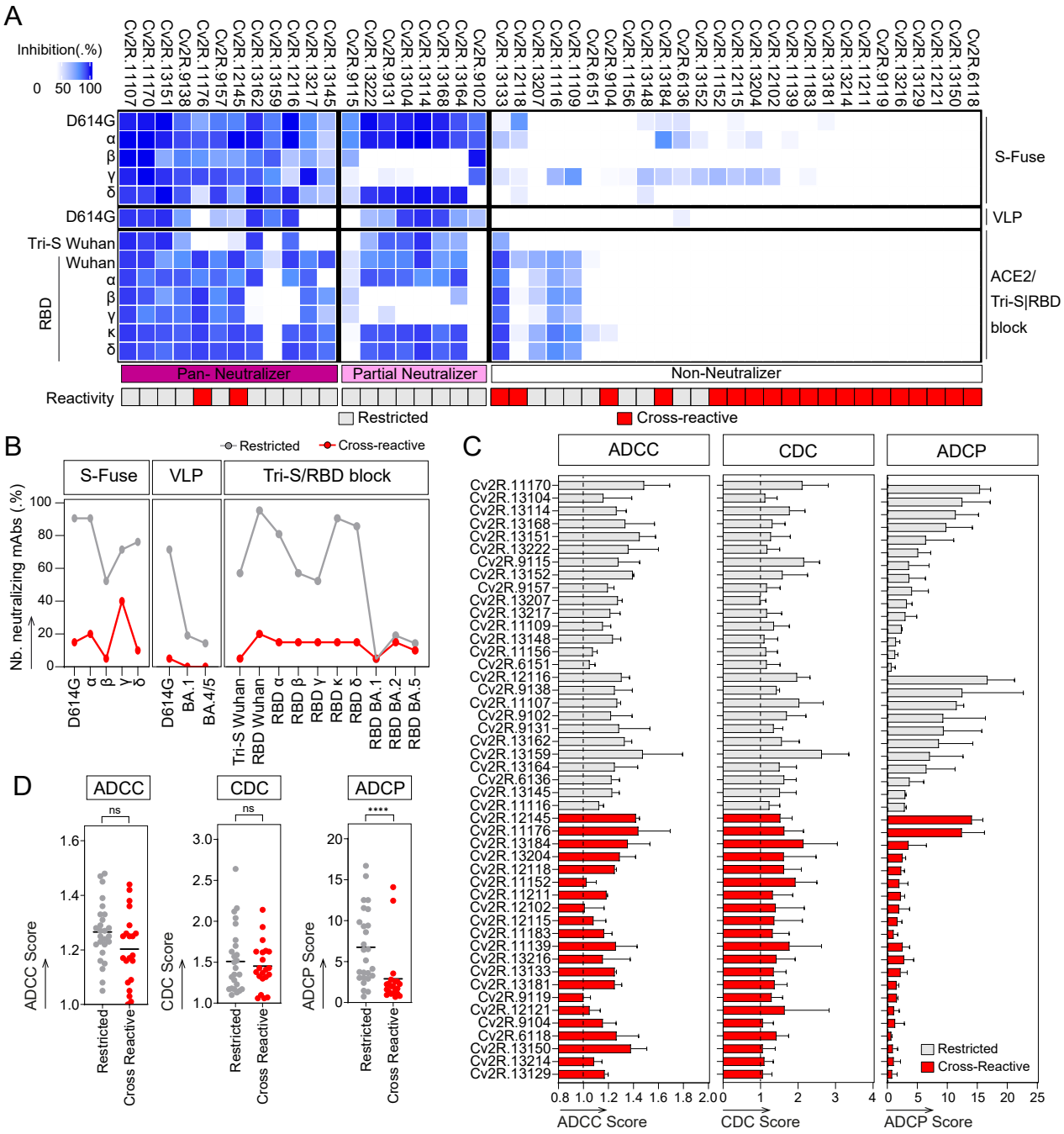
A
Inhibition(.%)
0 50 100
D614G
α
β
γ
δ
D614G
Tri-S Wuhan
Wuhan
RBD
α
β
γ
κ
δ
S-Fuse
VLP
ACE2/
Tri-S|RBD
block
Pan- Neutralizer
Partial Neutralizer
Non-Neutralizer
Reactivity
Restricted
Cross-reactive
B
Restricted
Cross-reactive
S-Fuse
VLP
Tri-S/RBD block
Nb. neutralizing mAbs (.%)
D614G
α
β
γ
δ
D614G
BA.1
BA.4/5
Tri-S Wuhan
RBD Wuhan
RBD α
RBD β
RBD γ
RBD κ
RBD δ
RBD BA.1
RBD BA.2
RBD BA.5
C
ADCC
CDC
ADCP
ADCC Score
CDC Score
ADCP Score
Restricted
Cross-Reactive
D
ADCC
CDC
ADCP
ns
ns
****
ADCC Score
CDC Score
ADCP Score
Restricted
Cross Reactive

Figure 4

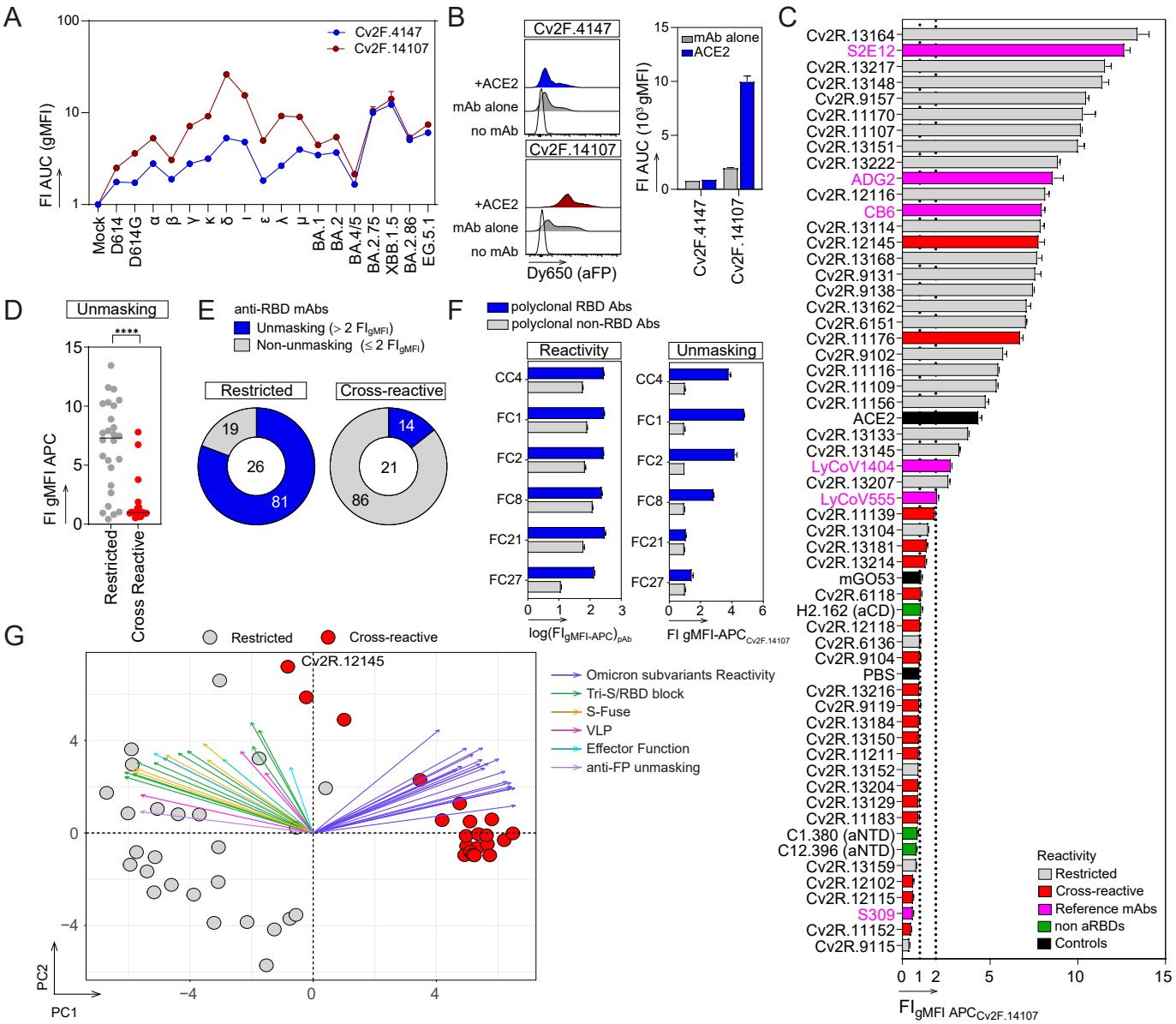
A
Cv2F.4147
Cv2F.14107
FI AUC (gMFI)
Mock
D614
D614G
α
β
γ
κ
δ
ι
ε
λ
μ
BA.1
BA.2
BA.4/5
BA.2.75
XBB.1.5
BA.2.86
EG.5.1
B
Cv2F.4147
Cv2F.14107
+ACE2
mAb alone
no mAb
Dy650 (aFP)
mAb alone
ACE2
FI AUC (10³gMFI)
C
Cv2R.13164
S2E12
Cv2R.13217
Cv2R.13148
Cv2R.9157
Cv2R.11170
Cv2R.11107
Cv2R.13151
Cv2R.13222
ADG2
Cv2R.12116
CB6
Cv2R.13114
Cv2R.12145
Cv2R.13168
Cv2R.9131
Cv2R.9138
Cv2R.13162
Cv2R.6151
Cv2R.11176
Cv2R.9102
Cv2R.11116
Cv2R.11109
Cv2R.11156
ACE2
Cv2R.13133
Cv2R.13145
LyCoV1404
Cv2R.13207
LyCoV555
Cv2R.11139
Cv2R.13104
Cv2R.13181
Cv2R.13214
mGO53
Cv2R.6118
H2.162 (aCD)
Cv2R.12118
Cv2R.6136
Cv2R.9104
PBS
Cv2R.13216
Cv2R.9119
Cv2R.13184
Cv2R.13150
Cv2R.11211
Cv2R.13152
Cv2R.13204
Cv2R.13129
Cv2R.11183
C1.380 (aNTD)
C12.396 (aNTD)
Cv2R.13159
Cv2R.12102
Cv2R.12115
S309
Cv2R.11152
Cv2R.9115
Reactivity
Restricted
Cross-reactive
Reference mAbs
non aRBDs
Controls
FI gMFI APC Cv2F.14107
D
Unmasking
FI gMFI APC
Restricted
Cross Reactive
E
anti-RBD mAbs
Unmasking (> 2 FI gMFI)
Non-unmasking (≤ 2 FI gMFI)
Restricted
Cross-reactive
19
26
81
14
21
86
F
polyclonal RBD Abs
polyclonal non-RBD Abs
Reactivity
Unmasking
CC4
FC1
FC2
FC8
FC21
FC27
log(FI gMFI-APC)pAb
FI gMFI-APC Cv2F.14107
G
Restricted
Cross-reactive
Cv2R.12145
Omicron subvariants Reactivity
Tri-S/RBD block
S-Fuse
VLP
Effector Function
anti-FP unmasking
PC1
PC2

Figure 5

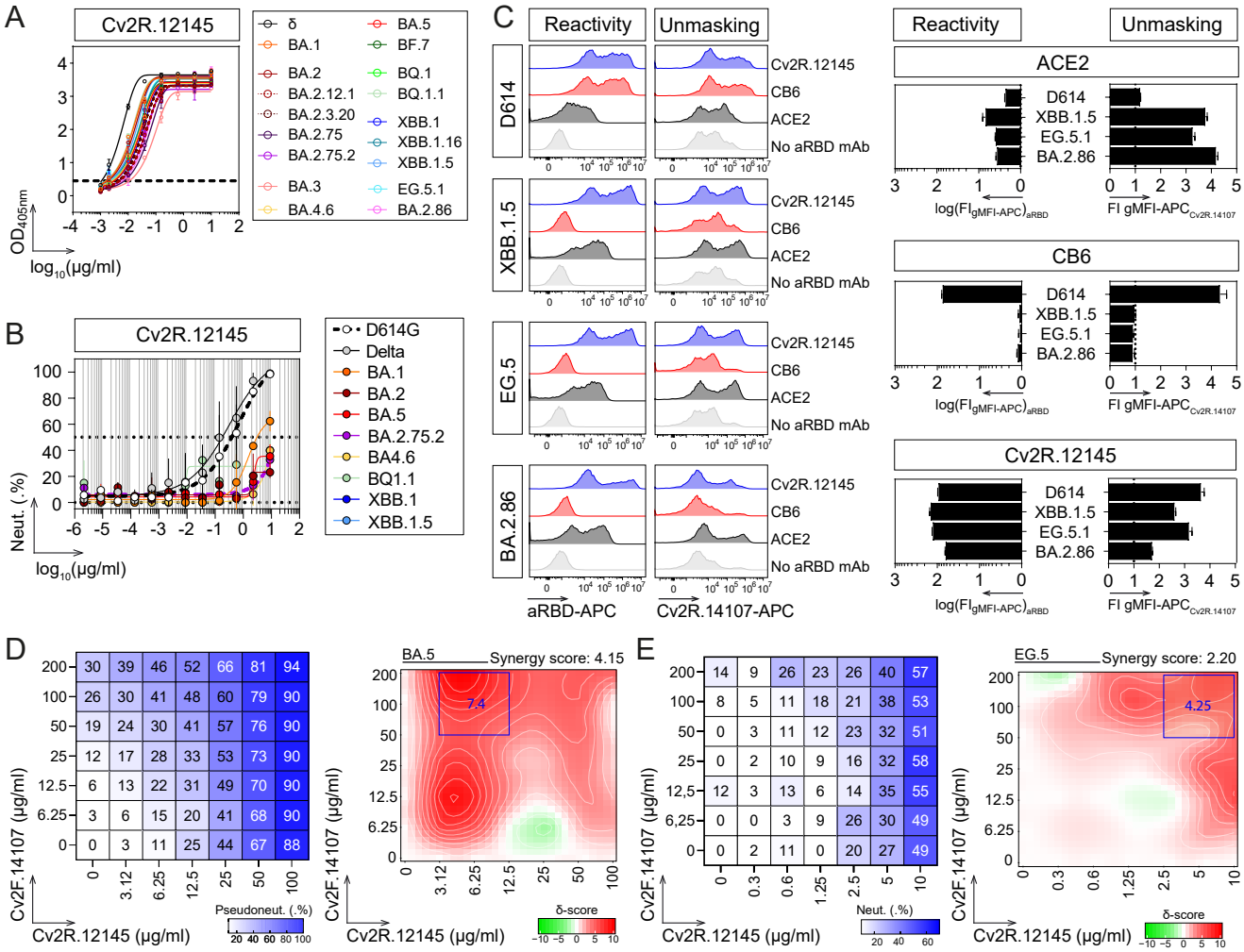
A
Cv2R.12145
OD405nm
log10(µg/ml)
δ
BA.1
BA.2
BA.2.12.1
BA.2.3.20
BA.2.75
BA.2.75.2
BA.3
BA.4.6
BA.5
BF.7
BQ.1
BQ.1.1
XBB.1
XBB.1.16
XBB.1.5
EG.5.1
BA.2.86
B
Cv2R.12145
Neut. (.%)
log10(µg/ml)
D614G
Delta
BA.1
BA.2
BA.5
BA.2.75.2
BA4.6
BQ1.1
XBB.1
XBB.1.5
C
Reactivity
Unmasking
D614
XBB.1.5
EG.5
BA.2.86
Cv2R.12145
CB6
ACE2
No aRBD mAb
aRBD-APC
Cv2R.14107-APC
Reactivity
Unmasking
ACE2
CB6
Cv2R.12145
D614
XBB.1.5
EG.5.1
BA.2.86
log(FIgMFI-APC)aRBD
FI gMFI-APCCv2R.14107
D
Cv2F.14107 (µg/ml)
Cv2R.12145 (µg/ml)
Pseudoneut. (.%)
BA.5
Synergy score: 4.15
7.4
δ-score
E
Neut. (.%)
EG.5
Synergy score: 2.20
4.25